iScience

CellPress
OPEN ACCESS

Article

The activation of LBH-CRYAB signaling promotes cardiac protection against I/R injury by inhibiting apoptosis and ferroptosis

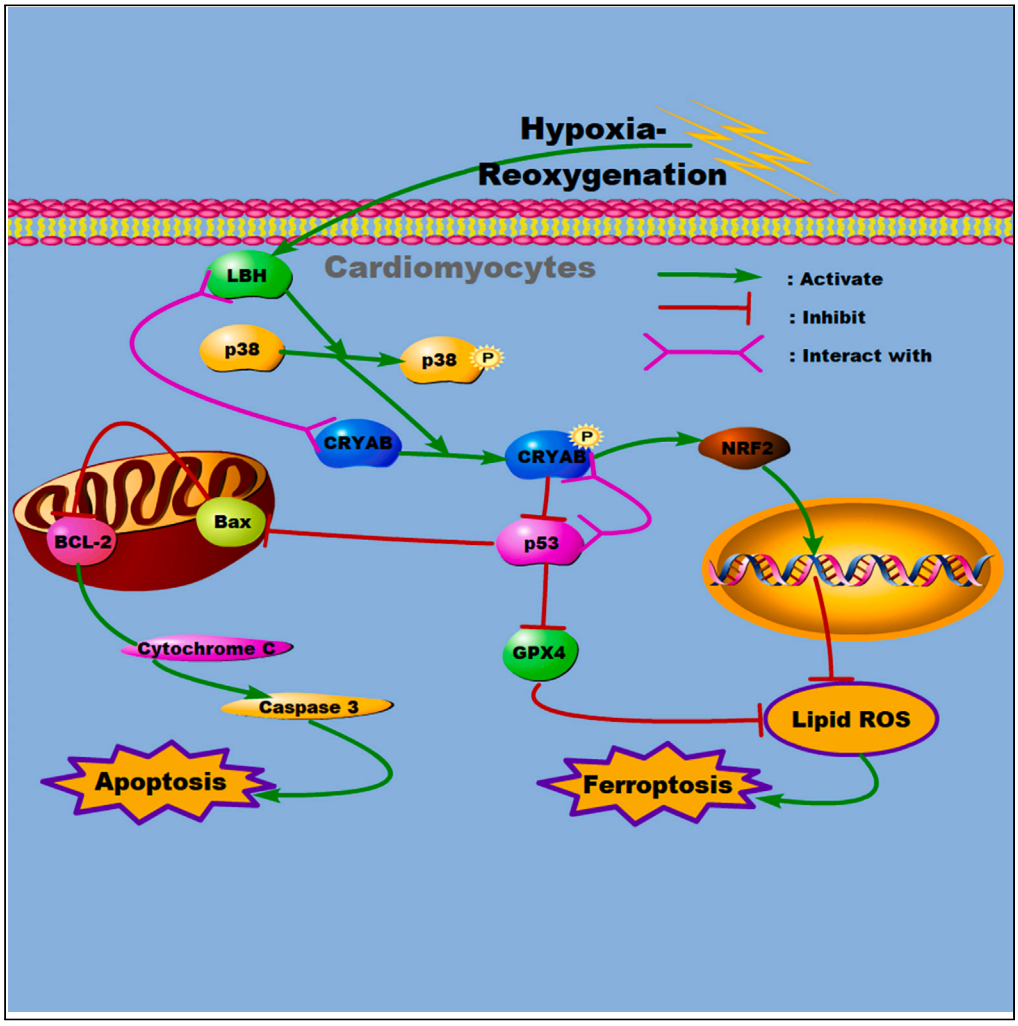

Anbiao Wu, Chongbin Zhong, Xudong Song, ..., Houda Huang, Pingzhen Yang, Qicai Liu

y_pingzhen@126.com (P.Y.)
liuqicai968@smu.edu.cn (Q.L.)

Highlights

LBH-CRYAB signaling is activated in damaged CMs during I/R injury

p53 is a mutual downstream effector for both LBH-inhibited apoptosis and ferroptosis

LBH overexpression *in vivo* exerts enhanced cardiac protection against I/R injury

Wu et al., iScience *27*, 109510
May 17, 2024
https://doi.org/10.1016/j.isci.2024.109510

iScience

CellPress
OPEN ACCESS

Article

The activation of LBH-CRYAB signaling promotes cardiac protection against I/R injury by inhibiting apoptosis and ferroptosis

Anbiao Wu,[1,2,4] Chongbin Zhong,[1,4] Xudong Song,[1] Wen Yuan,[3] Mintian Tang,[3] Tao Shu,[1] Houda Huang,[1] Pingzhen Yang,[1,*] and Qicai Liu[1,5,*]

SUMMARY

Myocardial ischemia-reperfusion (I/R) injury stands out among cardiovascular diseases, and current treatments are considered unsatisfactory. For cardiomyocytes (CMs) in ischemic tissues, the upregulation of Limb-bud and Heart (LBH) and αB-crystallin (CRYAB) and their subsequent downregulation in the context of cardiac fibrosis have been verified in our previous research. Here, we focused on the effects and mechanisms of activated LBH-CRYAB signaling on damaged CMs during I/R injury, and confirmed the occurrence of mitochondrial apoptosis and ferroptosis during I/R injury. The application of inhibitors, ectopic expression vectors, and knockout mouse models uniformly verified the role of LBH in alleviating both apoptosis and ferroptosis of CMs. p53 was identified as a mutual downstream effector for both LBH-CRYAB-modulated apoptosis and ferroptosis inhibition. In mouse models, LBH overexpression was confirmed to exert enhanced cardiac protection against I/R-induced apoptosis and ferroptosis, suggesting that LBH could serve as a promising target for the development of I/R therapy.

INTRODUCTION

Despite various diagnostic and therapeutic improvements in recent years, cardiovascular diseases remain to be the leading cause of current death globally, among which ischemic heart disease accounts for approximately half of the dead cases.[1] Specifically, ischemia is caused by the occlusion of the coronary artery; when the occlusion is cleared and the blood supply into the ischemic myocardium is restored, additional damage is inflicted on the ischemic myocardium by this reperfusion.[2] The entire process is defined as myocardial I/R injury, which has been characterized by numerous experimental and clinical evidences.[2–4] The corresponding treatments for myocardial I/R injury, however, have been limited and unsatisfactory due to the relatively fast disease progression and complicated pathogenic factors, including metabolic alterations, reactive oxygen species (ROS) overproduction, inflammation, autophagy dysregulation and mitochondrial dysfunction.[5,6] Besides, ever since been raised,[7] the timely reperfusion has been the first-line treatment for acute myocardial infarction (MI) to limit infarct and reduce mortality.[8,9] Thus, the molecular mechanisms of reperfusion injury need to be further deciphered to determine potential therapeutic strategies.

The Limb-bud and Heart (LBH) gene is a highly conserved transcriptional cofactor specifically expressed in the embryonic limb and heart.[10] In embryonic development, aberrant LBH expression during normal cardiogenesis leads to congenital heart disease[11]; we first examined expressional changes of LBH in cardiomyocytes (CMs) and cardiac fibroblasts (CFs) located in the peri-infarct areas after MI, as well as its role in regulating the profibrotic differentiation of CFs through the p38-αB-crystallin (CRYAB) axis.[12,13] During post-MI fibrosis, the initial activation of LBH-CRYAB signaling under hypoxia and the subsequent attenuation in prolonged process of collateral recruitment were observed in CMs.[13] This trend hinted the potential participation of LBH in regulating myocardial I/R injury, during which the injured CMs also experienced hypoxia-reoxygenation (H/R).

Various types of CM death during myocardial I/R injuries have been extensively studied, including necroptosis, mitochondrial apoptosis, mitochondrial necrosis, autophagy, ferroptosis, pyroptosis, parthanatos, and so forth.[14] Characterized by nuclear condensation, cell shrinkage and DNA fragmentation,[15,16] mitochondrial apoptosis was the first identified mode of programmed CM death in the pathogenesis of I/R injury.[14] Moreover, since it was defined a decade ago,[17] ferroptosis has been frequently reported to be involved in I/R injuries in multiple organs as a novel type of iron-dependent regulated cell death[18] and has been considered a promising therapeutic target for many

[1]Guangdong Provincial Biomedical Engineering Technology Research Center for Cardiovascular Disease, Sino-Japanese Cooperation Platform for Translational Research in Heart Failure, Laboratory of Heart Center, Department of Cardiology, Zhujiang Hospital, Southern Medical University, Guangzhou 510280, People's Republic of China
[2]Beijing Institute of Basic Medical Sciences, Beijing 100850, People's Republic of China
[3]Experimental Animal Center, Zhujiang Hospital, Southern Medical University, Guangzhou 510280, People's Republic of China
[4]These authors contributed equally
[5]Lead contact
*Correspondence: y_pingzhen@126.com (P.Y.), liuqicai968@smu.edu.cn (Q.L.)
https://doi.org/10.1016/j.isci.2024.109510

cardiovascular diseases, including myocardial I/R injury.[19] The regulatory mechanisms of ferroptosis can be generally divided into three categories: the SLC7A11-GSH-GPX4 pathway, the p62-Keap1-NRF2 pathway and the regulation of iron metabolism,[20] all of which result in augmented phospholipid peroxidation and the final ferroptosis. Heat shock proteins (HSPs) have been widely reported to participate in ferroptosis *in vivo* and *in vitro*,[21] among which CRYAB/HSP20 have been demonstrated to modulate both mitochondrial apoptosis[22,23] and ferroptosis.[24,25]

In our preliminary experiment with mice subjected to I/R surgery, synchronous expressional changes of LBH, phosphorylated-CYRAB, and NRF2 were discovered, as well as gradually increasing p53 levels and apoptotic and ferroptotic indicators in injured heart tissues. Based on these results and the reported findings described above, we aimed to explore the exact effects of LBH-CRYAB signaling on the regulation of multiple mechanisms of CM death during myocardial I/R injury and the potential downstream effectors corresponding to these CM death mechanisms.

RESULTS

Limb-bud and heart and *p*-αB-crystallin underwent synchronous upregulation and reduction during ischemia-reperfusion injury in a mouse model

Our previous studies have revealed the initial activation and subsequent attenuation of LBH-CRYAB cascades in both CMs and CFs during post-MI fibrosis.[12,13] Here, we intended to check the dynamic expression of LBH and *p*-CRYAB (Ser59) during I/R-induced myocardial injury. Based on the results, at both the mRNA and protein levels, LBH expression in mouse heart was upregulated by ischemia, peaked at the early stage of reperfusion, and then was downregulated during prolonged reperfusion (Figures 1A–1C and S1), which was also the case of I/R-injured rat hearts (Figure S2). The spread of TUNEL positive signals into risk areas and increased iron/MDA concentrations detected in ischemic areas might imply the exacerbation of apoptosis and ferroptosis[26,27] during prolonged reperfusion (Figures 1A and 1D). Therefore, the expression of NRF2 and p53 was also measured; the enhanced p53 expression and declined NRF2 expression at the end of reperfusion were consistent with these findings (Figures 1B, 1C, and S3). Noticeably, the levels of *p*-CRYAB and NRF2 also exhibited synchronous changes compared to LBH expression (Figures 1A–1C and S1). All these data prompted the potential relationship between activated LBH-CRYAB signaling and possible apoptosis and ferroptosis during I/R-induced myocardial injury.

Limb-bud and heart and *p*-αB-crystallin are upregulated and subsequently diminished during hypoxia-reoxygenation-induced myocardial apoptosis

The myocardium consists of different cell types; thus, *in vitro* experiments were conducted on both primary CMs and CM lines to confirm the expressional changes measured in heart tissues. At both the mRNA and protein levels, the expression of LBH and NRF2 underwent on the initial upregulation and subsequent downregulation in primary CMs and H9c2 cells under H/R treatment (Figures 2A–2C), during which upregulated LBH was observed to translocate into the nucleus in H9c2 cells (Figure 2D). The phosphorylation of p38 and CRYAB, together with HIF-1α expression, manifested similar variation trends during H/R, while the protein levels of total p38 and CRYAB remained stable in primary CMs and H9c2 cells (Figures 2B and 2C). In addition, the WB results indicated gradually ascending protein levels of cleaved Caspase3 and Bax/Bcl-2 ratios in both primary CMs and H9c2 cells (Figures 2B and 2C), which indicated an increase in mitochondrial apoptosis.[15,28]

Ectopic limb-bud and heart expression protects cardiomyocytes from apoptosis induced by hypoxia-reoxygenation

To further verify the role of LBH-CRYAB cascades in modulating CM apoptosis under H/R conditions, CMs with ectopic LBH expression were applied to assays testing cellular viability and apoptosis. LBH-overexpressed H9c2 cells exhibited higher viabilities after H/R treatment, and LBH-knockdown decreased the viabilities of both primary CMs and H9c2 cells after H/R treatment (Figures 3A, 3B, and S4). Correspondingly, LBH overexpression caused mitigated apoptosis ratios compared to the negative control, while LBH silencing promoted apoptosis in primary CMs, HL1 cells, and H9c2 cells during the entire H/R process, according to TUNEL staining and Annexin V/7-AAD flow cytometry (Figures 3C, 3D, and S5A–S5C). Therefore, we concluded that LBH-CRYAB signaling protects CMs from H/R-induced apoptosis.

p38-αB-crystallin signaling is activated by limb-bud and heart and participates in limb-bud and heart-induced myocardial protection against apoptosis

We reported that LBH regulates CRYAB phosphorylation at Ser59 via modulating p38 phosphorylation in nasopharyngeal carcinoma[29]; the phosphorylated p38-mediated Ser59 CRYAB phosphorylation was initially discovered in neuroscience studies.[30,31] The immunoblotting results showed the bidirectional correlation between LBH-mediated p38-CRYAB signaling and mitochondrial apoptotic biomarkers (p53, cleaved caspase3 and Bax/Bcl-2 ratios) in both LBH-overexpressed and LBH-silenced CMs and HL1 cells during H/R treatment (Figures 4A–4C, S6, and S5D). Thus, the p38 phosphorylation inhibitor ralimetinib was introduced to explore the potential relationship between LBH-activated p38 phosphorylation and CM apoptosis. From the WB results, enhanced H/R-induced cleaved Caspase3 levels and Bax/Bcl-2 ratios in p38 phosphorylation-inhibited CMs validated our assumption (Figure 4D), indicating that LBH-mediated myocardial protection against H/R-induced apoptosis was partially implemented through p38-CRYAB signaling, which is effectuated by phosphorylation activation.

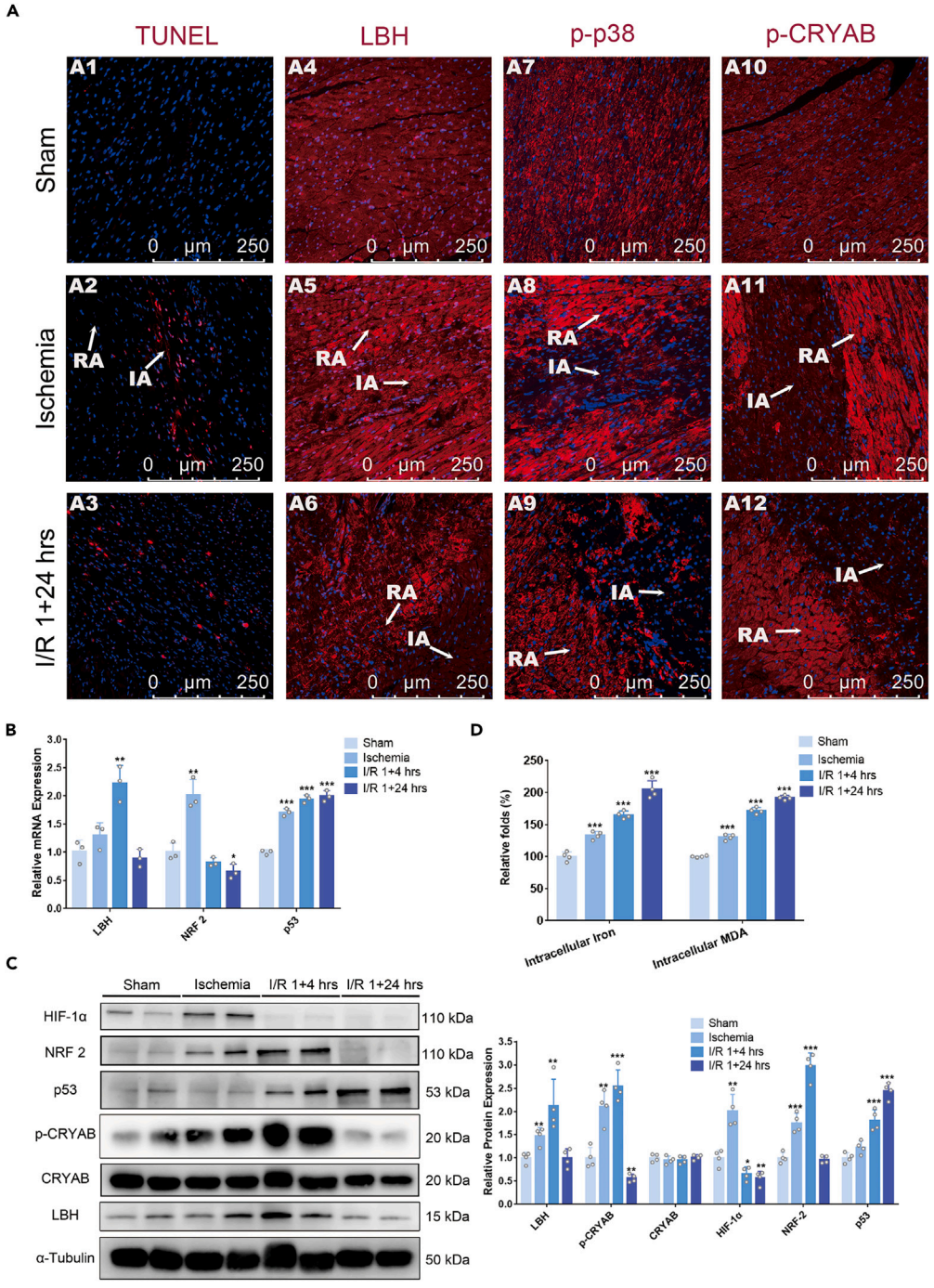

Figure 1. LBH and *p*-CRYAB underwent upregulation and subsequent attenuation during ischemia-reperfusion injury in a mouse model

(A) Cross-sections of hearts from the sham and I/R groups at the indicated time points after surgery were stained with TUNEL, anti-LBH, anti-p-p38 or anti-*p*-CRYAB (infarct areas and CMs in ischemic risk areas are indicated by white arrows). The mRNA levels of LBH, p53, and NRF2 (B) and protein expression of HIF-1*α*, LBH, *p*-CRYAB, CRYAB, p53 and NRF2 (C) in ischemic heart tissue at the indicated time points after surgery (Brown-Forsythe ANOVA test, * = $p < 0.05$, ** = $p < 0.01$ and *** = $p < 0.001$ vs. Sham. Error bars are mean ± SD).

(D) Relative iron and MDA concentrations measured in ischemic heart tissue at the indicated time points after surgery (Brown-Forsythe ANOVA test, * = $p < 0.05$, ** = $p < 0.01$ and *** = $p < 0.001$ vs. Sham. Error bars are mean ± SD).

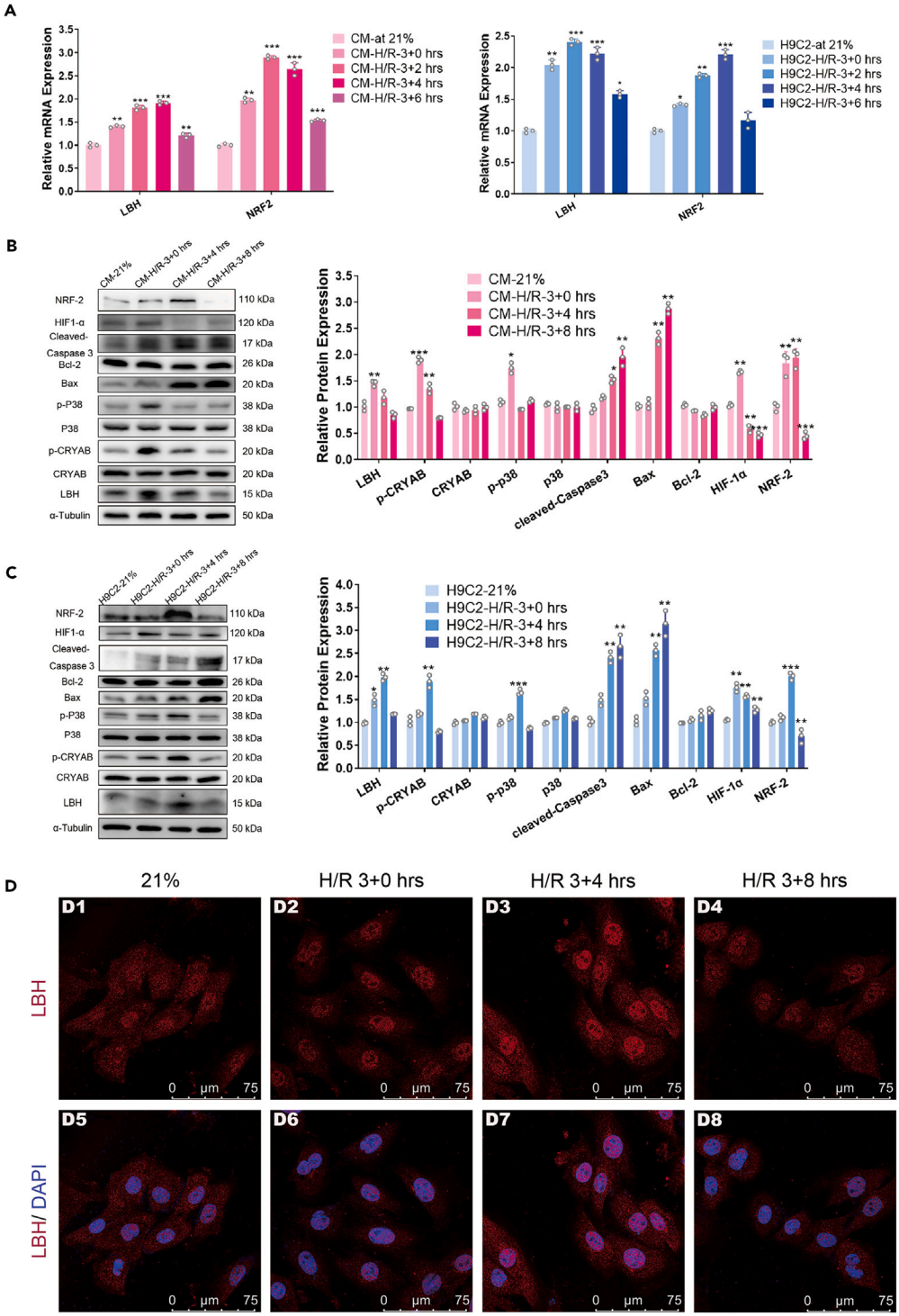

Figure 2. LBH and *p*-CRYAB were upregulated and subsequently doregulated during the hypoxia-reoxygenation process in myocardial cells

The mRNA levels of LBH and CRYAB (A) and protein expression of HIF-1α, LBH, p-p38, p-38, *p*-CRYAB, CRYAB, Bax, Bcl-2 and cleaved-Caspase 3 in primary mouse CMs (B) and H9c2 cells (C) at different time points during H/R treatment (Brown-Forsythe ANOVA test, * = $p < 0.05$, ** = $p < 0.01$ and *** = $p < 0.001$ vs. 21%. Error bars are mean ± SD).

(D) Representative immunofluorescence images of H9c2 cells stained with anti-LBH at different time points during H/R treatment.

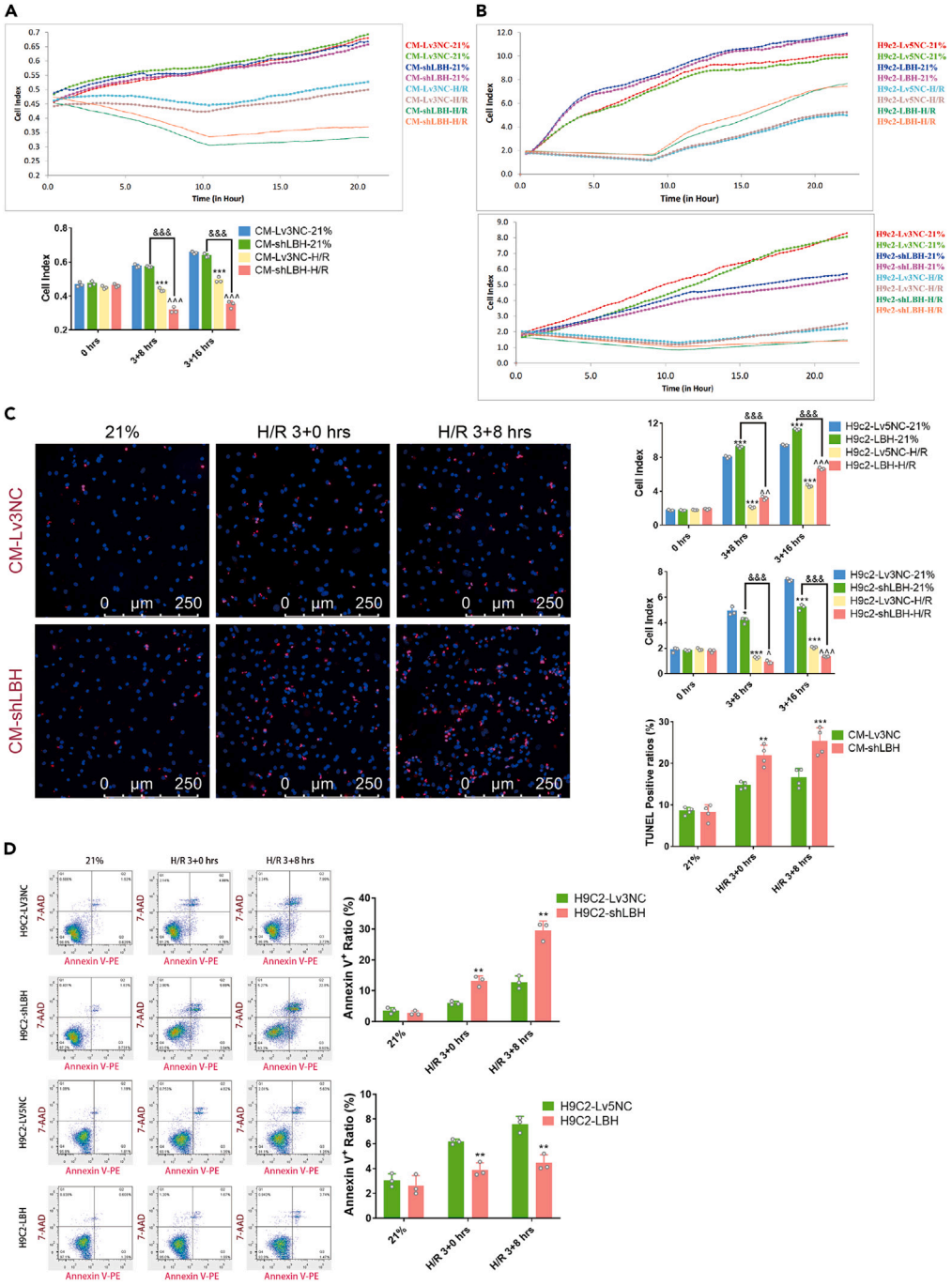

Figure 3. LBH knockdown worsens myocardial apoptosis induced by hypoxia-reoxygenation

Cellular viabilities of lentivirus-infected primary mouse CMs (A) and H9c2 cells (B) under H/R treatment (Brown-Forsythe ANOVA test, *** = $p < 0.001$ vs. CM-NC-21% or H9c2-NC-21%; $^{\&\&}$ = $p < 0.01$ and $^{\&\&\&}$ = $p < 0.01$ for shLBH-21% vs. shLBH-H/R or LBH-21% vs. LBH-H/R; ^^^ = $p < 0.001$ for Lv3-NC-H/R vs. shLBH-H/R or Lv5-NC-H/R vs. LBH-H/R. Error bars are mean ± SD).

(C) Cellular apoptosis in lentivirus-infected primary mouse CMs under H/R treatment, as indicated by TUNEL staining (Unpaired t-test with Welch's correction, ** = $p < 0.01$ and *** = $p < 0.001$ vs. Lv3-NC. Error bars are mean ± SD).

(D) Cellular apoptosis in lentivirus-infected primary H9c2 cells under H/R treatment, as indicated by Annexin V/7-AAD flow cytometry (Unpaired t-test with Welch's correction, ** = $p < 0.01$ vs. Lv3-NC or Lv5-NC. Error bars are mean ± SD).

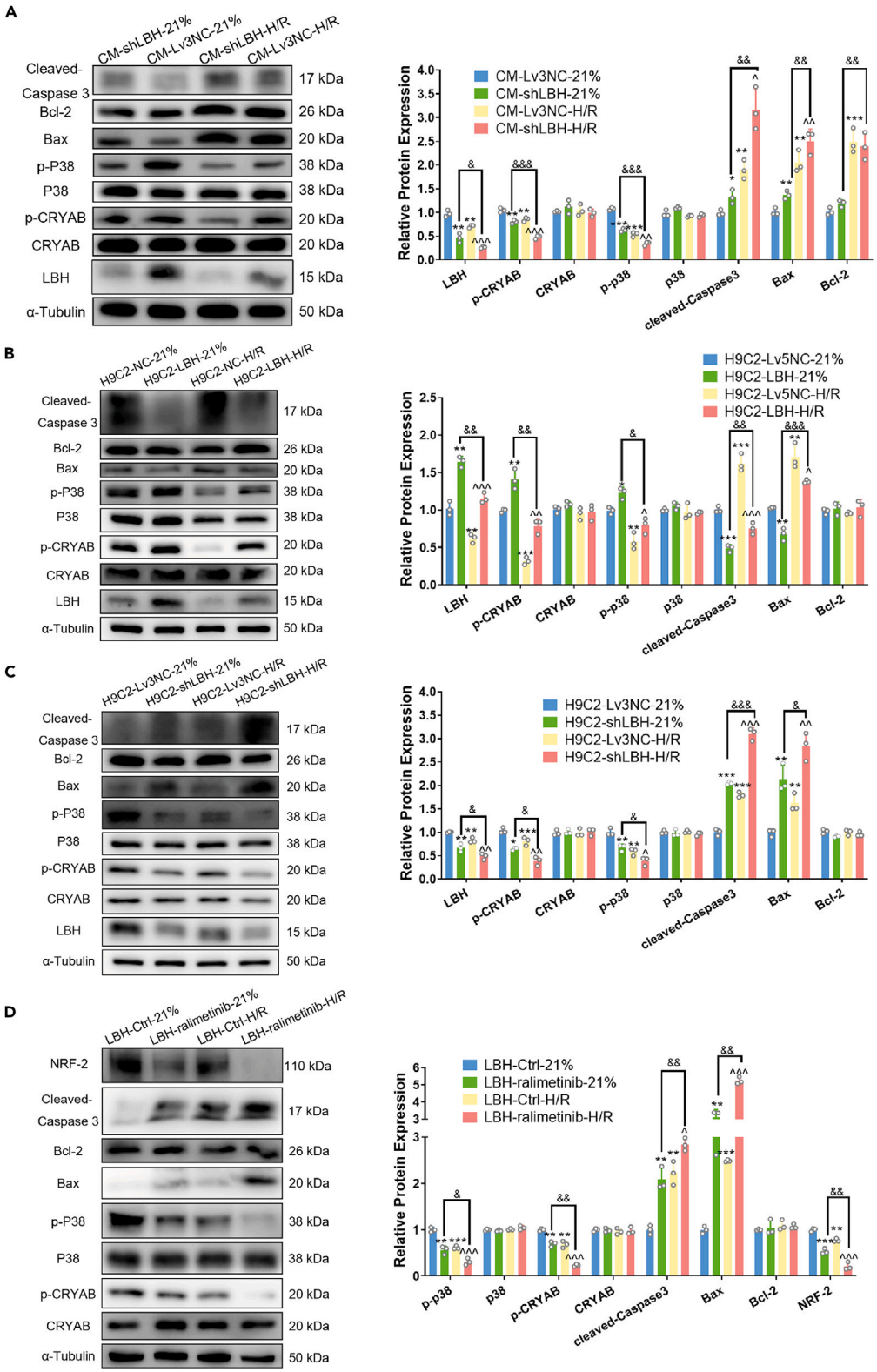

Figure 4. p38-CRYAB signaling is involved in LBH-induced myocardial protection against apoptosis

Protein expression of LBH, p-p38, p-38, *p*-CRYAB, CRYAB, Bax, Bcl-2 and cleaved-Caspase 3 in primary mouse CMs (A) transiently overexpressing LBH or in stable LBH-overexpressing (B) and LBH-silenced (C) H9c2 cells (Brown-Forsythe ANOVA test, * = $p < 0.05$, ** = $p < 0.01$ and *** = $p < 0.001$ vs. Lv3-NC-21% or

Figure 4. *Continued*

Lv5-NC-21%; $^{\&}$ = $p < 0.05$, $^{\&\&}$ = $p < 0.01$ and $^{\&\&\&}$ = $p < 0.01$ for Lv3-shLBH-21% vs. Lv3-shLBH-H/R or Lv5-LBH-21% vs. Lv5-LBH-H/R; ^ = $p < 0.05$, ^^ = $p < 0.01$ and ^^^ = $p < 0.001$ for Lv3-NC-H/R vs. Lv3-shLBH-H/R or Lv5-NC-H/R vs. Lv5-LBH-H/R. Error bars are mean ± SD).

(D) Protein expression of NRF2, *p*-CRYAB, CRYAB, p-p38, p-38, Bax, Bcl-2, and cleaved-Caspase 3 in stable LBH-overexpressing H9c2 cells with or without ralimetinib treatment (Brown-Forsythe ANOVA test, ** = $p < 0.01$ and *** = $p < 0.001$ vs. LBH-Ctrl-21%; ^ = $p < 0.05$ and ^^^ = $p < 0.001$ for LBH-Ctrl-H/R vs. LBH-Inhibitor-H/R; $^{\&}$ = $p < 0.05$ and $^{\&\&}$ = $p < 0.01$ for LBH-Inhibitor-21% vs. LBH-Inhibitor-H/R. Error bars are mean ± SD).

Apoptosis and ferroptosis are involved in limb-bud and heart knockout-augmented myocardial injury during ischemia-reperfusion

Because the detected LBH-mediated apoptotic effects on CMs (Figures 3A and 3C) did not account for all the cell death under H/R treatment and ferroptosis was observed in I/R models (Figure 1D), whether LBH participate in modulating ferroptosis during the I/R process requires our investigation. After LBH^{KO} mice were applied to I/R surgery, LBH knockout was found to further aggravate cardiac dysfunction (indicated by ECG) and myocardial injury (indicated by TTC staining) after I/R treatment (Figures 5A and 5B). Accordingly, increased apoptosis and ferroptosis were discovered in LBH^{KO} I/R models, as indicated by TUNEL staining and iron/MDA measurement (Figures 5C and 5D); similar results were observed in H/R-injured H9c2 cells in response to apoptosis inhibitor or ferroptosis inhibitor treatment (Figure S7C). In addition, the protein levels of p-p38, *p*-CRYAB, NRF2, and GPX4 were also diminished in the ischemic heart tissue of LBH^{KO} mice after surgery, together with elevated p53 expression (Figures 5E and S8), which were also consistent with the changes in protein expression in H/R-treated CMs with ectopic LBH expression (Figures 4A–4C). Collectively, we concluded that apoptosis and ferroptosis were simultaneously involved in LBH-mediated myocardial protection under I/R or H/R conditions.

Ectopic limb-bud and heart expression mediates ferroptosis in cardiomyocytes during hypoxia-reoxygenation treatment

Hence, the potential function of the LBH gene in mediating ferroptosis in H/R-treated CMs was also tested *in vitro*. Iron/MDA measurement and FerroOrange staining uniformly demonstrated gradually increasing ferroptosis in both primary CMs and H9c2 cells during the H/R process (Figures 6A and 6B), which is also in line with NRF2 expressional changes (Figures 2B and 2C). Furthermore, H/R-induced ferroptosis was enhanced in LBH^{KO} CMs compared to negative controls, while LBH-overexpressed H9c2 cells exhibited attenuated ferroptosis after H/R treatment (Figures 6C and 6D). Considering that multiple mechanisms are involved in H/R-induced myocardial cell death,[14] the ferroptosis inducer erastin[32] was introduced to specifically mimic ferroptosis during the H/R process, and similar results were obtained in both LBH^{KO} CMs and LBH-overexpressed H9c2 cells in iron and MDA measurements (Figure 6C). Additionally, LBH overexpression and knockdown in HL1 cells were found not to affect the H/R-induced autophagy and necroptosis, as indicated by the immunoblotting of corresponding biomarkers (Figure S9). These results suggested that LBH upregulation protects CMs against H/R-induced ferroptosis and erastin-induced ferroptosis.

Limb-bud and heart-mediated p38-αB-crystallin signaling restrains p53 expression and erastin-induced ferroptosis in cardiomyocytes

CRYAB has been thought to participate in the ferroptosis regulation of cancer cells by bioinformatics researches.[24,25] Based on the results described above, the possible relationship between LBH-activated p38-CRYAB signaling and LBH-regulated myocardial protection against ferroptosis was investigated. In LBH^{WT} primary CMs, erastin treatment increased the levels of LBH, *p*-CRYAB and NRF2, as well as the diminished expression of Keap1 and GPX4,[33] which implies ongoing LBH-mediated resistance to ferroptosis (Figure 7A). The changing trends of *p*-CRYAB, NRF2, Keap1 and GPX4 were significantly reversed in LBH^{KO} CMs, indicating the exacerbation of erastin-induced ferroptosis due to LBH knockout (Figure 7A). Then, ralimetinib was applied to CMs under erastin treatment to examine the role of phosphorylated p38. We found that inhibiting p38 phosphorylation also significantly reversed the upregulation of LBH, *p*-CRYAB, NRF2, and the downregulation of Keap1 and GPX4 under erastin treatment, together with elevated p53 expression (Figure 7B). What is more, CRYAB-overexpressed CMs were also subjected to erastin treatment, and the results showed further promoted the upregulation of *p*-CRYAB, NRF2, and downregulation of Keap1 and GPX4, together with decreased p53 expression (Figure 7C), which was consistent with attenuated erastin-induced ferroptosis in CRYAB-overexpressed CMs (Figure 7D). In conclusion, LBH-mediated myocardial protection against ferroptosis was partially achieved by LBH-activated p38-CRYAB signaling, which inhibited p53 expression.

Limb-bud and heart-αB-crystallin activation is associated with enhanced nuclear factor-erythroid factor 2 expression, intranuclear translocation and ferroptosis inhibition in cardiomyocytes

In ferroptotic signal transduction, NRF2 has been reported to function by transcriptionally regulating heme oxygenase-1 (HO-1) expression[20]; thus, in addition to cytoplasmic NRF2 protein levels, its intranuclear distribution was also examined. NRF2 translocation into the nucleus was found to be augmented with erastin treatment (Figures 8A and 8B); LBH-overexpressed H9c2 presented higher intranuclear LBH and NRF2 levels than negative controls, which is in line with the amelioration of cell injury in H9c2-LBH cells induced by erastin treatment (Figures 8A and 8B). Besides, CRYAB overexpression increased *p*-CRYAB, GPX4 and decreased p53 levels in erastin-treated AC16 cells compared to AC16-Scramble cells (Figure 8C). Accordingly, AC16-CRYAB cells showed alleviated erastin-induced ferroptosis compared to negative controls, as indicated by iron/MDA measurement and FerroOrange staining conformably (Figures 8D and 8E). Altogether, p53 downregulation induced by the LBH-CRYAB axis synchronized with enhanced NRF2 expression and nuclear translocation, and inhibited myocardial ferroptosis.

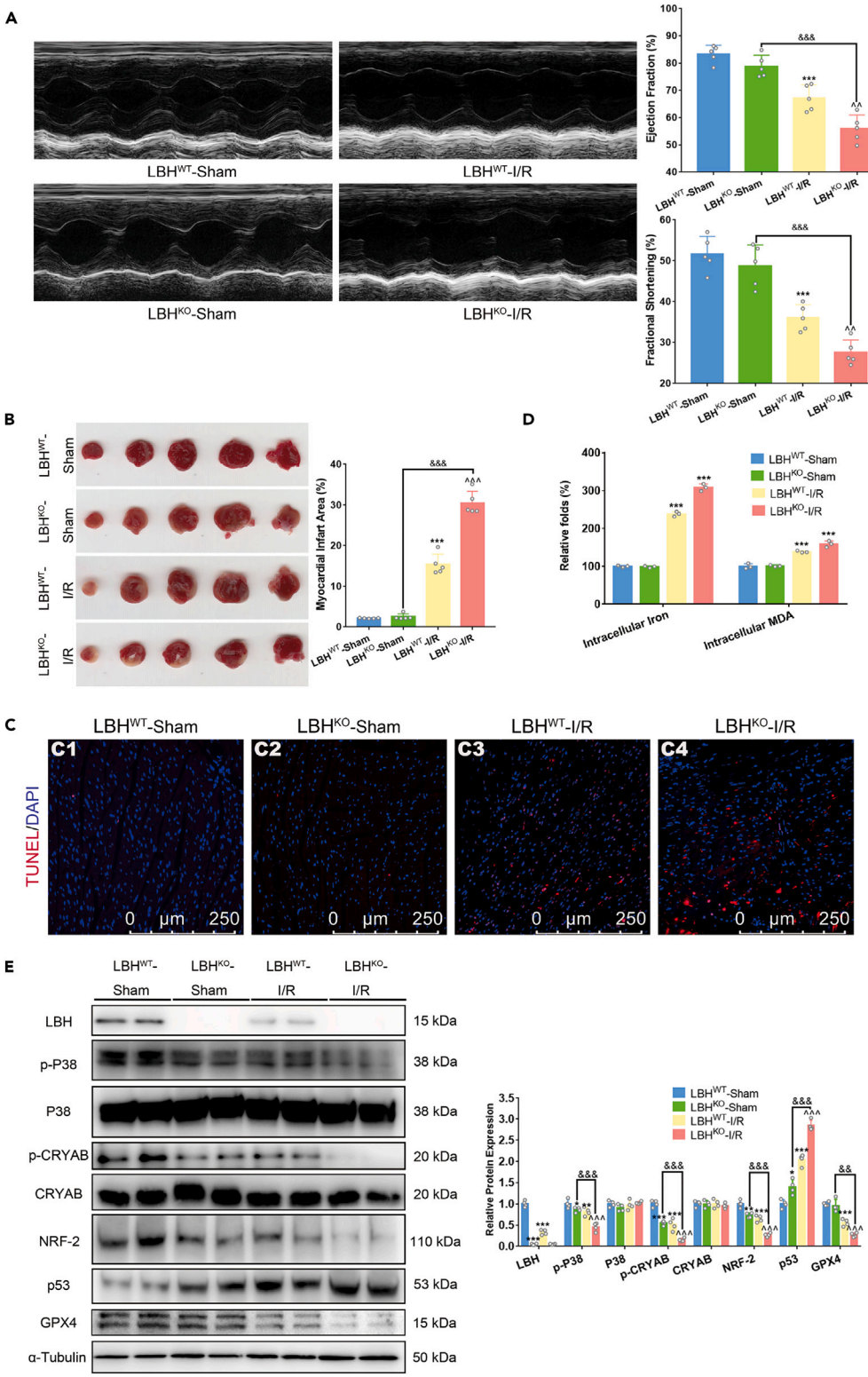

Figure 5. LBH knockout aggravates cardiac dysfunction induced by ischemia-reperfusion injury, during which both apoptosis and ferroptosis are involved

(A) Representative echocardiograms of LBH^{WT}-Sham, LBH^{KO}-Sham, LBH^{WT}-I/R, and LBH^{KO}-I/R mice and the corresponding statistical analysis of cardiac EFs and FSs (Brown-Forsythe ANOVA test, *** = $p < 0.001$ vs. LBH^{WT}-Sham; $^{\&\&\&}$ = $p < 0.001$ vs. LBH^{KO}-Sham; ^^ = $p < 0.01$ vs. LBH^{WT}- I/R. Error bars are mean ± SD).

Figure 5. *Continued*

(B) Representative TTC staining of heart cross-sections of LBH^{WT}-Sham, LBH^{KO}-Sham, LBH^{WT}-I/R, and LBH^{KO}-I/R mice and the corresponding statistical analysis of myocardial infarct areas indicated by the staining (Brown-Forsythe ANOVA test, *** = $p < 0.001$ vs. LBH^{WT}-Sham; $^{\&\&\&}$ = $p < 0.001$ vs. LBH^{KO}-Sham; ^^^ = $p < 0.001$ vs. LBH^{WT}- I/R. Error bars are mean ± SD).

(C) Representative TUNEL staining of heart cross-sections of LBH^{WT}-Sham, LBH^{KO}-Sham, LBH^{WT}-I/R, and LBH^{KO}-I/R mice.

(D) Relative iron and MDA concentrations measured in the ischemic heart tissue of LBH^{WT}-Sham, LBH^{KO}-Sham, LBH^{WT}-I/R, and LBH^{KO}-I/R mice (Brown-Forsythe ANOVA test, *** = $p < 0.001$ vs. LBH^{WT}-Sham; $^{\&\&\&}$ = $p < 0.001$ vs. LBH^{KO}-Sham; ^^^=<0.001 vs. LBH^{WT}- I/R. Error bars are mean ± SD).

(E) Protein expression of LBH, p-p38, p38, *p*-CRYAB, CRYAB, p53, KEAP-1 and NRF2 in ischemic heart tissue of LBH^{WT} mice/LBH^{KO} mice after surgery (Brown-Forsythe ANOVA test, * = $p < 0.05$, ** = $p < 0.01$ and *** = $p < 0.001$ vs. LBH^{WT}-Sham; $^{\&\&}$ = $p < 0.01$ and $^{\&\&\&}$ = $p < 0.001$ vs. LBH^{KO}-Sham; ^^^ = $p < 0.001$ vs. LBH^{WT}-I/R. Error bars are mean ± SD).

The limb-bud and heart-αB-crystallin axis affects p53 signaling via both protein-protein interactions with *p*-αB-crystallin and p53 transcriptional regulation

p53 has been reported to participate in various mechanisms regulating cellular ferroptosis[34]; moreover, Deng et al.[35] stated that LBH-CRYAB signaling, after being activated through PPI, regulates the transcriptional activity of p53. Consequently, the negative correlation between LBH-CRYAB signaling and p53 expression observed in CMs under H/R or Erastin treatment raised our interest. Phosphor-CRYAB (Ser59) was proven to interact with the p53 protein in myogenic cells[36]; our results showed that p53 and phosphor-CRYAB proteins were colocalized in the nucleuses of primary mouse CMs and AC16 cells (Figure 9A). After ZDOCK calculation revealed that human p53 and CRYAB proteins formed a stable protein docking model (Figure S10), the phosphor-CRYAB protein in primary mouse CMs and Ac16 cells were confirmed to interact with p53 protein, according to FRET and co-IP assays (Figures 9B, 9C, and 9D). Finally, the luciferase reporter assay presented elevated p53 transcriptional activities in LBH knockdown or H/R-treated AC16 cells compared to negative controls (Figure 9E), which suggests that the LBH-CRYAB axis might affect p53 signaling via both PPIs and LBH-CRYAB-mediated transcriptional regulation.

Limb-bud and heart rescue in limb-bud and heart^{KO} mice partially restores cardiac protection against myocardial injury induced by ischemia-reperfusion

After detecting intensified I/R-induced myocardial injury in LBH^{KO} mice, we decided to bidirectionally prove the role of the LBH gene by re-expressing LBH in knockout mice before performing I/R surgery. The data demonstrated that LBH rescue partially alleviated cardiac dysfunction and myocardial injury after I/R treatment (Figures 10A and 10B). Additionally, both I/R-induced apoptosis and ferroptosis were significantly dampened by LBH rescue (Figures 10C and 10D), which was in also accordance with the upregulation of *p*-CRYAB, NRF2, GPX4 and downregulation of p53 in the heart tissues of LBH^{KO}-Rescued-I/R mice compared to those of LBH^{KO}-NC-I/R mice (Figures 10E and S11). LBH-mediated restoration of cardiac protection against I/R injury confirmed the role of LBH in preventing cardiac dysfunction during I/R process by affecting both apoptosis and ferroptosis.

Limb-bud and heart overexpression in limb-bud and heart wild type^{WT} mice enhances cardiac protection against ischemia-reperfusion injury

Apart from apoptosis, ferroptosis has received increasing attention for its potential as a therapeutic target, especially in cardiovascular diseases.[19,37] Therefore, we explored the translational potentials of LBH-associated therapy on ameliorating I/R injury by introducing exogenous expressional vectors of LBH into wild type mice. Abnormal LBH overexpression in LBH^{WT} mice (Figure 11A) was discovered to diminish cardiac dysfunction and myocardial injury compared to mice with background LBH levels (Figures 11B and 11C), including the mitigation of both apoptosis and ferroptosis (Figures 11D and 11E). That is, presurgical LBH overexpression in LBH^{WT} mice enhanced cardiac protection against I/R-induced apoptosis and ferroptosis.

DISCUSSION

The rapid course and complex pathogenesis of I/R injury make proper treatment rather challenging among cardiovascular disease therapies, during which various types of programmed cell death need to be addressed. Therefore, our exploration of the corresponding molecular mechanisms to mitigate I/R injury might prefer the potential targets that are activated quickly and involved in different pathways. We pioneered the research of LBH in cardiovascular diseases by revealing its role in modulating post-MI cardiac fibrosis through activating the p38-CRYAB axis in CFs.[12] Since similar expressional changes were also observed in CMs within ischemic areas after MI,[13] the relationship between LBH and CRYAB phosphorylation activated by phosphorylated p38 in damaged CMs during myocardial I/R injury required our examination. In heart tissue slices, the presence and gradual expansion of apoptosis and ferroptosis during the I/R process were affirmed; to exclude possible interference initiated by other cell types, primary CMs and H9c2 cells were also subjected to H/R treatment to mimic the reduced blood and oxygen supply received by the ischemic myocardium. The results at both *in vivo* and *in vitro* levels conformably exhibited the initial elevation and subsequent decrease of LBH, p-p38, and *p*-CRAYB during the whole course of I/R and H/R, accompanied by the up-regulation of biomarkers of mitochondrial apoptosis, which suggest that the activation of LBH-CRYAB signaling might contribute to CM survival, while its attenuation leads to the obliteration of this protective effect against apoptosis.

The abnormal phosphorylation of CRYAB at Ser59 has been reported to be associated with the aging of the myocardium and the occurrence of cardiomyopathy.[38] In this study, ectopic LBH expression was introduced into both primary CMs and H9c2 cells for the detections of

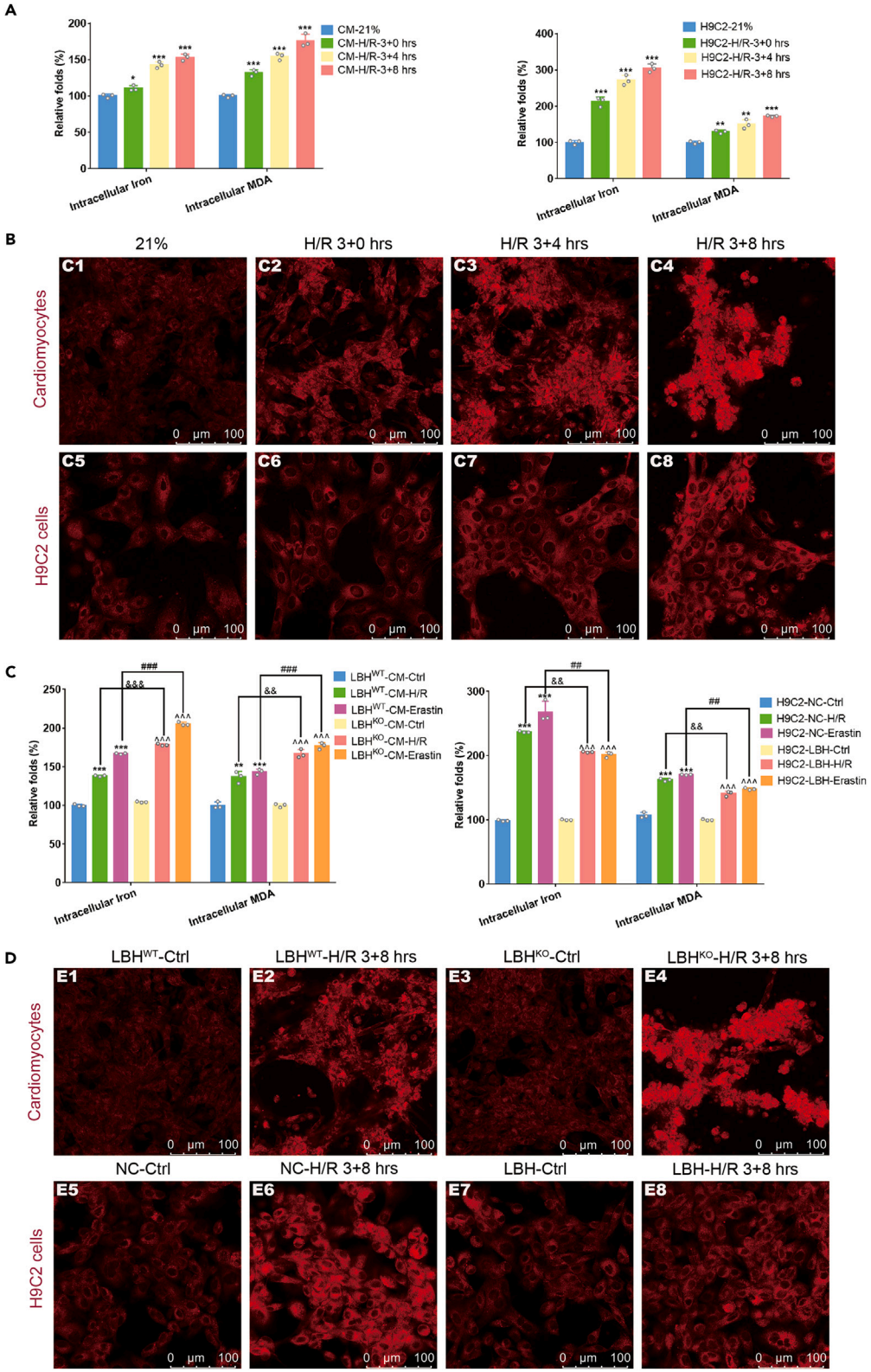
A
Relative folds (%)
CM-21%
CM-H/R-3+0 hrs
CM-H/R-3+4 hrs
CM-H/R-3+8 hrs
Intracellular Iron
Intracellular MDA
H9C2-21%
H9C2-H/R-3+0 hrs
H9C2-H/R-3+4 hrs
H9C2-H/R-3+8 hrs
B
21%
H/R 3+0 hrs
H/R 3+4 hrs
H/R 3+8 hrs
Cardiomyocytes
H9C2 cells
C1
C2
C3
C4
C5
C6
C7
C8
0 μm 100
C
LBHWT-CM-Ctrl
LBHWT-CM-H/R
LBHWT-CM-Erastin
LBHKO-CM-Ctrl
LBHKO-CM-H/R
LBHKO-CM-Erastin
H9C2-NC-Ctrl
H9C2-NC-H/R
H9C2-NC-Erastin
H9C2-LBH-Ctrl
H9C2-LBH-H/R
H9C2-LBH-Erastin
D
LBHWT-Ctrl
LBHWT-H/R 3+8 hrs
LBHKO-Ctrl
LBHKO-H/R 3+8 hrs
NC-Ctrl
NC-H/R 3+8 hrs
LBH-Ctrl
LBH-H/R 3+8 hrs
E1
E2
E3
E4
E5
E6
E7
E8

Figure 6. Ectopic LBH expression mediates ferroptosis in cardiomyocytes during hypoxia-reoxygenation treatment

(A) Relative iron and MDA concentrations measured in mouse CMs/H9c2 cells under H/R treatment (Brown-Forsythe ANOVA test, *** = $p < 0.001$ vs. CM/H9c2-21%. Error bars are mean ± SD).

(B) FerroOrange staining in live mouse CMs/H9c2 cells under H/R treatment.

(C) Relative iron and MDA concentrations measured in mouse CMs/H9c2 cells with ectopic LBH expression under H/R or Erastin treatment (Brown-Forsythe ANOVA test, *** = $p < 0.001$ vs. LBH^{WT-}Ctrl/H9c2-NC-Ctrl; ^^^ = $p < 0.001$ vs. LBH^{KO-}Ctrl/H9c2-LBH-Ctrl; && = $p < 0.01$, &&& = $p < 0.001$ vs. LBH^{WT-}H/R or H9c2-NC-H/R; ## = $p < 0.01$, ### = $p < 0.001$ vs. LBH^{WT-}Erastin/H9c2-NC-Erastin. Error bars are mean ± SD).

(D) FerroOrange staining in live mouse CMs/H9c2 cells with ectopic LBH expression under H/R treatment.

protein expression, apoptotic assay and apoptotic biomarkers; the corresponding results uniformly confirmed that LBH enhances the phosphorylation of p38 and CRYAB, inhibits mitochondrial apoptosis in CMs under hypoxia-reoxygenation and vice versa. In addition, the introduction of the p38 phosphorylation inhibitor abolished the increase in CRYAB phosphorylation at Ser59 induced by LBH overexpression and caused exacerbated pro-apoptotic biomarkers in CMs under H/R conditions. These results implied that LBH-modulated cardiac protection against H/R-induced apoptosis is effectuated by p38-CRYAB cascades, which is also in line with our previous findings about LBH-p38-CRYAB signaling in nasopharyngeal carcinoma.[39]

To further explore the role of the LBH gene during the I/R process, we constructed the LBH^{KO} mouse model. The analysis of injured size, cardiac function, TUNEL staining, and the expression of apoptotic biomarkers congruously illustrated that conventional LBH knockout augmented apoptosis-associated myocardial injury in mice suffering from the I/R process. Meanwhile, ferroptosis was detected in LBH^{WT} mice; here, LBH knockout was found to enhance I/R-induced ferroptosis, which prompted us to investigate the function of LBH in regulating H/R-related ferroptosis *in vitro*. Notably, NRF2 is considered a critical factor regulating oxidative stress responses and ferroptosis[18,40] while expression correlations between CRYAB and NRF2 were discovered in cancer study.[40] Generally, NRF2 was believed to be activated under oxidative conditions,[41] playing the central role in maintaining the redox balance and resisting ferroptosis through p62-keap1-NRF2 signaling[42] to subsequently regulate the transcription of oxidoreductases and oxygenases such as HO-1,[43] while NRF2 upregulation was also found to affect the SLC7A11-GPX4 pathway during ferroptosis.[44] For myocardial I/R injuries, NRF2 expression has been shown to be closely related to ferroptosis progression in CMs under H/R conditions, while GPX4 serves as the terminal effector that directly regulates lipid-ROS generation.[45] In this study, bidirectional LBH ectopic expression in CMs verified the function of LBH in ameliorating both H/R-induced and erastin-induced ferroptosis, as indicated by the expression of NRF2 and GPX4. Besides, chloroquine diphosphate and ferrostatin-1 were separately applied to CMs at effective concentrations; the fact that H/R injury in CMs was partially reversed by either inhibitor testified the coexistence of H/R-induced apoptosis and ferroptosis in CMs. Specifically, for the restraint of CM ferroptosis, designated expressional regulation of LBH, p-p38, and *p*-CRYAB was executed in consecutive order, and the data showed that LBH-mediated ferroptosis restriction shared the same molecular mechanisms as apoptotic regulation, which was mediated by p38 phosphorylation and following CRYAB phosphorylation. In addition, NRF2 expression is regulated by LBH-CRYAB signaling and presented a similar variation trend in CMs, namely upregulation under hypoxia followed by downregulation during reoxygenation, which could be viewed as the activation of ferroptosis resistance and its gradual decay. This finding is also consistent with that of Fittipaldi et al.,[46] who stated that the activation of p38 phosphorylation triggered by disrupted redox homeostasis promoted both the expression and phosphorylation of CRYAB, which leads to NRF2 upregulation and apoptosis resistance; and that of Mitra et al.,[47] in which the treatment of p38 inhibitor led to the decreased activation of CRYAB and NRF2, together with increased mitochondrial apoptotic load detected in a rat MI model.

Moreover, p53 expression was observed to be negatively correlated with LBH-CRYAB signaling under I/R or H/R conditions. Previous studies have revealed the relationship between CRYAB activation and p53 expression. In detail, CRYAB reduces the mitochondrial translocation of p53 and therefore inhibits p53-mediated apoptosis through PPIs in C2C12 cells under ROS-generated oxidative stress.[36] On the other hand, p53 was also reported to transcriptionally regulate CRYAB during apoptotic progression, while CRYAB was also reported to interact with the p53 DNA-binding domain, influence p53 transcription and inhibit p53-dependent apoptosis, according to different researches.[45,48–50] In our study, the luciferase reporter assay confirmed that p53 was upregulated at the mRNA level by LBH knockdown or H/R treatment in CMs; also, PPIs between p53 and *p*-CRYAB were verified. That is, CRYAB could inhibit p53 signaling in CMs by both means, leading to diminished p53-dependent mitochondrial apoptosis during hypoxia-reoxygenation,[48,51] which is strictly regulated by the activation of the caspase family and the release of proapoptotic elements from damaged mitochondria, such as cytochrome *c*.[16]

Compared to that of apoptosis, the role of p53 expression in ferroptosis would be highly context dependent, since p53 was found to participate in ferroptosis regulation via various effectors, including SLC7A11, GLS2, SAT1/ALOX15, ALOX12, PTGS2, FDXR, and so forth,[52,53] which inflicted both pro-ferroptotic and anti-ferroptotic functions. Thus, the overall effect of p53 signaling on ferroptosis regulation is highly cell/tissue-type and stress signal specific.[53] The most frequently discussed ferroptotic mechanism of p53 regulation involves the SLC7A11-GSH-GPX4 pathway, in which GPX4 serves as the terminal effector[54–56]; while NRF2-mediated survival response has also been reported to be inhibited by p53 activation in the prolonged phase of oxidative stress.[57] In this study, p53 upregulation observed after the deactivation of LBH-CRYAB signaling was coherently correlated with promoted ferroptosis 24 h after reperfusion, as indicated by Fe^{2+}/MDA measurements and GPX4 expression. It is noteworthy that the upregulation of LBH, p-p38 p-CRYAB, and p53 was observed after erastin treatment and at the early phase of reperfusion (I/R 1 + 4 h). It is our understanding that these data refer to the LBH-mediated ferroptosis resistance after the activation of LBH-CRYAB signaling under hypoxia, while other potential factors might also participate in p53-modulated ferroptosis. Based on the fact that LBH knockout caused p53 upregulation, GPX4 downregulation, and aggravated ferroptosis in I/R-treated mice (I/R 1 + 24 h), LBH-overexpressing vectors were applied to constructed LBH^{KO} mice for further investigation. The data showed that LBH rescue led to

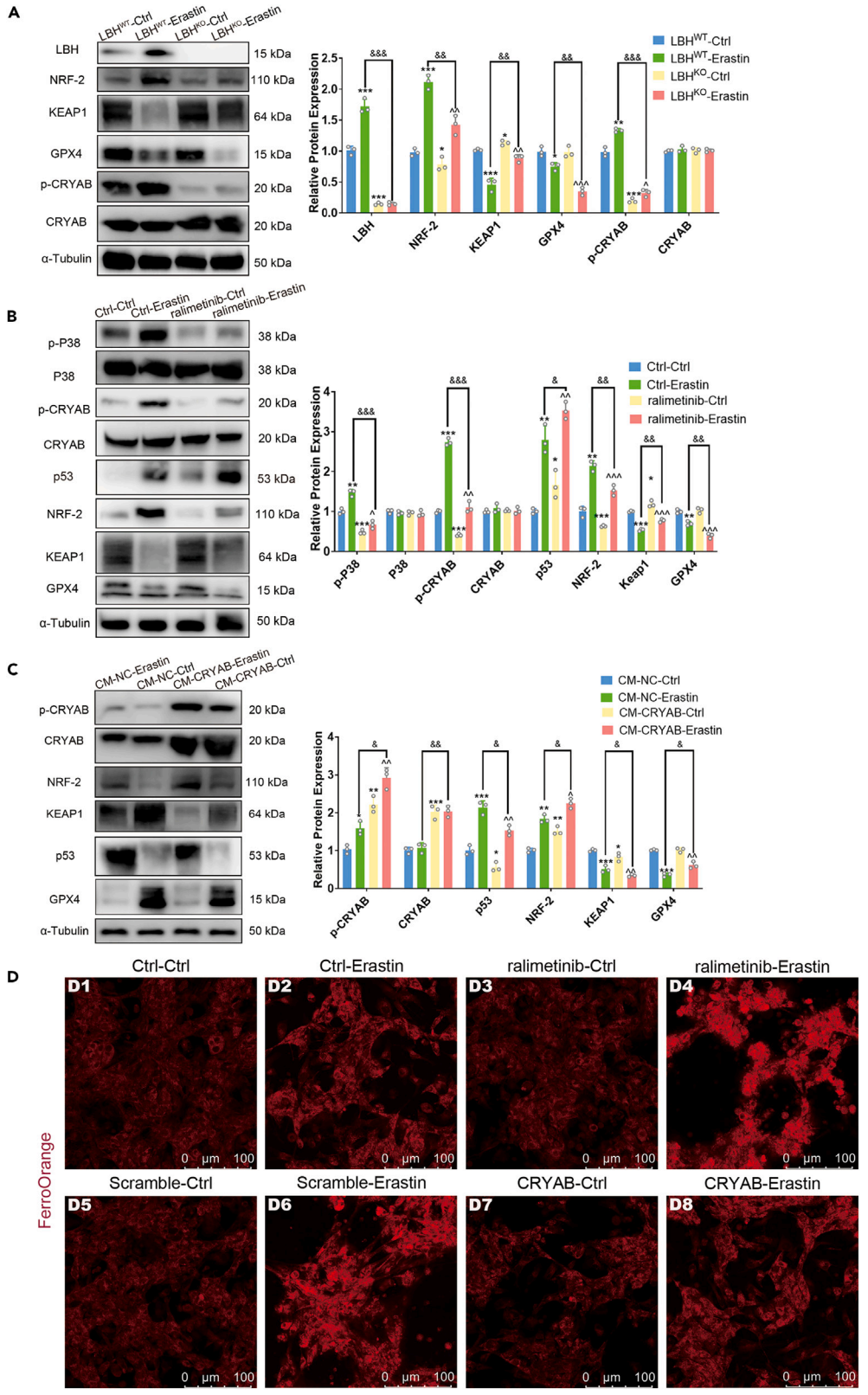
A
LBH^WT-Ctrl
LBH^WT-Erastin
LBH^KO-Ctrl
LBH^KO-Erastin
LBH
NRF-2
KEAP1
GPX4
p-CRYAB
CRYAB
α-Tubulin
15 kDa
110 kDa
64 kDa
15 kDa
20 kDa
20 kDa
50 kDa
Relative Protein Expression
LBH
NRF-2
KEAP1
GPX4
p-CRYAB
CRYAB
B
Ctrl-Ctrl
Ctrl-Erastin
ralimetinib-Ctrl
ralimetinib-Erastin
p-P38
P38
p-CRYAB
CRYAB
p53
NRF-2
KEAP1
GPX4
α-Tubulin
38 kDa
38 kDa
20 kDa
20 kDa
53 kDa
110 kDa
64 kDa
15 kDa
50 kDa
Relative Protein Expression
p-P38
P38
p-CRYAB
CRYAB
p53
NRF-2
Keap1
GPX4
C
CM-NC-Erastin
CM-NC-Ctrl
CM-CRYAB-Erastin
CM-CRYAB-Ctrl
p-CRYAB
CRYAB
NRF-2
KEAP1
p53
GPX4
α-Tubulin
20 kDa
20 kDa
110 kDa
64 kDa
53 kDa
15 kDa
50 kDa
Relative Protein Expression
p-CRYAB
CRYAB
p53
NRF-2
KEAP1
GPX4
D
Ctrl-Ctrl
Ctrl-Erastin
ralimetinib-Ctrl
ralimetinib-Erastin
FerroOrange
D1
D2
D3
D4
Scramble-Ctrl
Scramble-Erastin
CRYAB-Ctrl
CRYAB-Erastin
D5
D6
D7
D8
0 μm 100

Figure 7. LBH-mediated p38-CRYAB signaling inhibits p53 expression and ferroptosis in cardiomyocytes

(A) Protein expression of LBH, *p*-CRYAB, CRYAB, KEAP-1, NRF2 and GPX4 in CMs isolated from LBH^{WT} and LBH^{KO} mice under erastin treatment (Brown-Forsythe ANOVA test, * = $p < 0.05$, ** = $p < 0.01$ and *** = $p < 0.001$ vs. LBH^{WT}-Ctrl; $^{\&\&}$ = $p < 0.01$, $^{\&\&\&}$ = $p < 0.001$ vs. LBH^{WT}-Erastin; ^ = $p < 0.05$, ^^ = $p < 0.01$ vs. LBH^{KO}-Ctrl. Error bars are mean ± SD).

(B) Protein expression of LBH, p-p38, p38, *p*-CRYAB, CRYAB, KEAP-1, NRF2 and GPX4 in primary mouse CMs under ralimetinib/erastin treatment (Brown-Forsythe ANOVA test, * = $p < 0.05$, ** = $p < 0.01$ and *** = $p < 0.001$ vs. Ctrl-Ctrl; $^{\&\&}$ = $p < 0.01$ and $^{\&\&\&}$ = $p < 0.001$ vs. Ctrl-Erastin; ^^ = $p < 0.01$ and ^^^ = $p < 0.001$ vs. ralimetinib-Ctrl. Error bars are mean ± SD).

(C) Protein expression of LBH, *p*-CRYAB, CRYAB, KEAP-1, NRF2 and GPX4 in CRYAB-overexpressed mouse CMs under erastin treatment (Brown-Forsythe ANOVA test, ** = $p < 0.01$, *** = $p < 0.001$ vs. Scramble-Ctrl; $^{\&}$ = $p < 0.05$, $^{\&\&}$ = $p < 0.01$ vs. Scramble-Erastin; ^ = $p < 0.05$, ^^ = $p < 0.01$ and ^^^ = $p < 0.001$ vs. CRYAB-Ctrl. Error bars are mean ± SD).

(D) FerroOrange staining in live mouse CMs with ralimetinib treatment or ectopic CRYAB expression under erastin-induced ferroptosis.

decreased p53 expression, the increased expression of NRF2 and GPX4, together with alleviated ferroptosis compared to those in LBH^{KO} mice administered with control vectors before surgery, which bidirectionally proved the protective effect of LBH-CRYAB-mediated p53 downregulation against ferroptosis during I/R injury. Similar to apoptosis, ferroptosis has long been viewed as a potential therapeutic target for I/R injury in cardiovascular research.[58–61] p53 activation has been attributed to exacerbating cardiac I/R injury, in which both apoptotic and ferroptotic mechanisms have been explored.[61–63] Our data described above have confirmed the consistent role of LBH-CRYAB mitigated p53 expression in inhibiting both apoptosis and ferroptosis, which makes it more likely to reduce potential compensatory effects in the future development of I/R injury therapies compared to other targets concerned with single mechanisms of I/R-induced programmed cell death.

Also, we explored the potentiality of introducing extraneous LBH for cardiac protection and injury therapies under I/R conditions. Due to the fast disease progression of I/R, recombinant LBH protein would be a better option than external expression vectors.[64,65] And the high expenses of clinically available recombinant proteins urged us to evaluate whether exceeding the physiological level of LBH would bring about therapeutic effects for I/R injury. Here, LBH-overexpressing vectors were administered to LBH^{WT} mice before surgery; the results showed that LBH overexpression ameliorated both I/R-induced apoptosis and ferroptosis through p53-and NRF2-related signaling. Hence, we hypothesized that the administration of recombinant LBH protein upon detecting ischemia might mitigate subsequent reperfusion injuries after percutaneous coronary intervention; further testification by developing applicable recombinant proteins could be our research orientation in the future.

Conclusion

Collectively, this study elucidated the role of the activation and subsequent diminution of LBH-CRYAB signaling in protecting the myocardium against ischemia-reperfusion injury by inhibiting apoptosis and ferroptosis. Briefly, upregulated LBH stimulated the phosphorylation of p38 and CRYAB in hypoxic CMs located in ischemic areas; p53 downregulation was modulated by phosphorylated CRYAB by PPIs and transcriptional inhibition, which accounts for dampened mitochondrial apoptosis and ferroptosis of CMs; phosphorylated CRYAB also facilitated the upregulation and intranuclear translocation of NRF2, which alleviated ferroptosis of CMs through transcriptional regulation. Since external LBH overexpression was proven to synchronously mitigate mitochondrial apoptosis and ferroptosis of CMs, LBH could be a potential therapeutic target for the future development of ischemia-reperfusion treatments such as recombinant proteins.

Limitations of the study

In addition to these results obtained on conventional LBH knockout model, the construction of a cell-specific knockout model, in which LBH expression is conditionally knocked out in adult mouse CMs, would help to further specify the effects of LBH-CRYAB-mediated p53 downregulation in CMs during I/R injury. For example, using the Cre-lox system, we could construct Myh6-icre/ERT2-LBH^{KO} mouse models,[66] in which the knockout of LBH would be effectuated only when tamoxifen was administered at the designated time point. Moreover, this conditional LBH knockout in CMs could be matched with CM-specific LBH rescue, such as the construction of adeno-associated virus vector AAV9-CTnT promoter-LBH.[67] We intend to implement these methods and research models in further investigation.

STAR★METHODS

Detailed methods are provided in the online version of this paper and include the following:

- KEY RESOURCES TABLE
- RESOURCE AVAILABILITY
  - Lead contact
  - Materials availability
  - Data and code availability
- EXPERIMENTAL MODEL AND STUDY PARTICIPANT DETAILS
  - Animal
- METHOD DETAILS
  - Echocardiography (ECG)

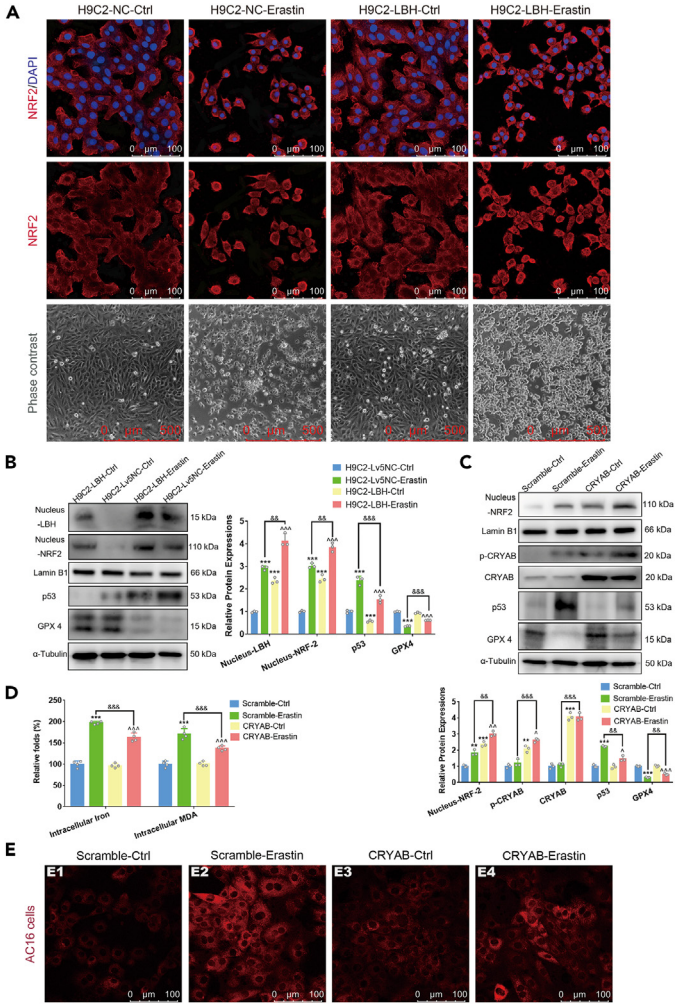

Figure 8. LBH-CRYAB signaling is associated with enhanced NRF-2 nuclear translocation and inhibited ferroptosis in cardiomyocytes

(A) Representative images of H9c2 cells for phase contrast imaging and immunostaining of NRF2 under erastin treatment.

(B) Western blotting testing the intranuclear LBH, NRF2 protein, together with p53 and GPX4 cytoplasmic levels in H9c2 cells under erastin treatment (Brown-Forsythe ANOVA test, *** = $p < 0.001$ vs. Lv5-NC-Ctrl; $^{\&\&\&}$ = $p < 0.001$ for LBH-Ctrl vs. LBH-Erastin; ^^ = $p < 0.01$ and ^^^ = $p < 0.001$ for Lv5-NC-Erastin vs. LBH-Erastin. Error bars are mean ± SD).

(C) Western blotting testing the intranuclear NRF2 protein, together with cytoplasmic levels of *p*-CRYAB, CRYAB, p53 and GPX4 in CYRAB-overexpressed AC16 cells under erastin treatment (Brown-Forsythe ANOVA test, ** = $p < 0.01$ and *** = $p < 0.001$ vs. Scramble-Ctrl; $^{\&\&}$ = $p < 0.01$ and $^{\&\&\&}$ = $p < 0.001$ for CRYAB-Ctrl vs. CRYAB-Erastin; ^ = $p < 0.05$ and ^^ = $p < 0.01$ for Scramble-Erastin vs. CRYAB-Erastin. Error bars are mean ± SD).

(D) Relative iron and MDA concentrations measured in CYRAB-overexpressed AC16 cells under erastin treatment (Brown-Forsythe ANOVA test, *** = $p < 0.001$ vs. Scramble-Ctrl; $^{\&\&\&}$ = $p < 0.001$ for CRYAB-Ctrl vs. CRYAB-Erastin; ^^^ = $p < 0.001$ for Scramble-Erastin vs. CRYAB-Erastin. Error bars are mean ± SD).

(E) FerroOrange staining in live CYRAB-overexpressed AC16 cells under erastin treatment.

- Isolation and culture of primary CMs
- Lentivirus infection and cell line culture
- Hypoxia-reoxygenation treatment
- Reagents and compounds
- Cellular viability assays
- Apoptosis detection
- Ferroptosis detection
- Quantitative real-time PCR
- Western blotting
- Protein-protein interaction (PPI)
- Immunofluorescence staining

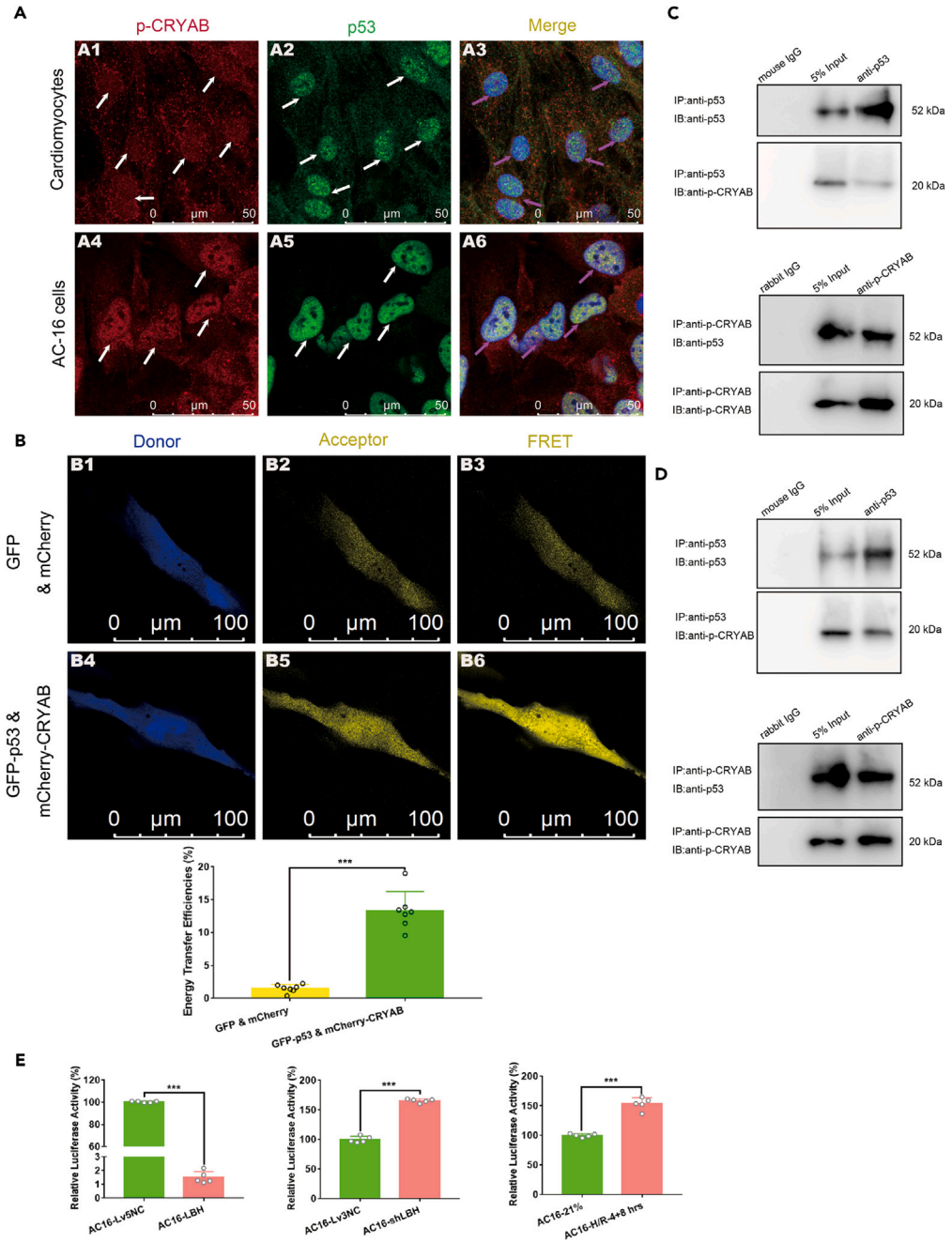

Figure 9. LBH expression affects the PPIs between *p*-CRYAB and p53 proteins and CRYAB-mediated p53 transcription

(A) Representative confocal microscopy images of *p*-CRYAB (red) and p53 (green) dual staining in mouse CMs and AC16 cells. The colocalizations in subcellular regions are indicated by white arrows.

(B) Representative images of plasmid-transfected AC16 cells obtained by the FRET-SE pattern on a Leica SP8 confocal microscope and the corresponding statistical analysis of the FRET efficiencies of co-transfected AC16 cells (Unpaired t-test with Welch's correction, *** = $p < 0.001$ vs. AC16-GFP&mCherry. Error bars are mean ± SD). PPIs between *p*-CRYAB and p53 in primary CMs (C) and Ac16 cells (D) were examined by immunoblotting (IB) after co-IP with anti-p53/anti-*p*-CRYAB antibodies.

(E) p53 transcriptional activity in established AC16 cell lines or Ac16 cells under H/R treatment as detected by luciferase reporter assays (Unpaired t-test with Welch's correction, *** = $p < 0.001$ vs. AC16-Lv3NC, AC16-Lv5NC or AC16-21%. Error bars are mean ± SD).

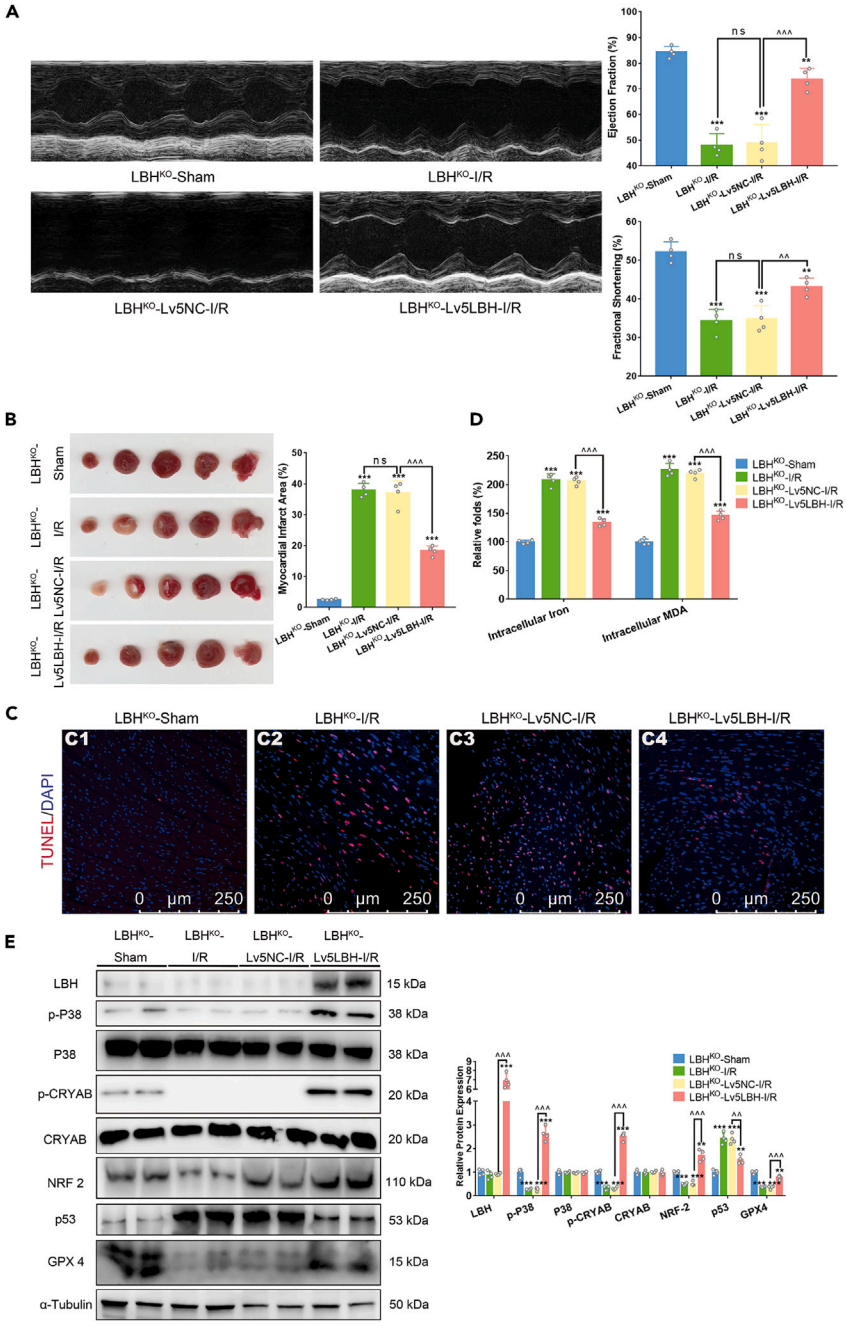

Figure 10. LBH rescue in LBH^{KO} mice restores part of the cardiac protection against cellular apoptosis, ferroptosis, and cardiac dysfunction induced by ischemia-reperfusion injury

(A) Representative echocardiograms of LBH^{WT}-Sham, LBH^{KO}-I/R, LBH^{KO}-Lv5NC-I/R and LBH^{KO}-LBH-I/R mice and the corresponding statistical analysis of cardiac EFs and FSs (Brown-Forsythe ANOVA test, *** = $p < 0.001$ vs. LBH^{WT}-Sham; ^^^ = $p < 0.001$ vs. LBH^{KO}-Lv5NC-I/R. Error bars are mean ± SD).

(B) Representative TTC staining of heart cross-sections of LBH^{WT}-Sham, LBH^{KO}-I/R, LBH^{KO}-Lv5NC-I/R and LBH^{KO}-LBH-I/R mice and the corresponding statistical analysis of myocardial infarct areas indicated by the staining (Brown-Forsythe ANOVA test, *** = $p < 0.001$ vs. LBH^{WT}-Sham; ^^ = $p < 0.01$, ^^^ = $p < 0.001$ vs. LBH^{KO}-Lv5NC-I/R. Error bars are mean ± SD).

(C) Representative TUNEL staining of heart cross-sections of LBH^{WT}-Sham, LBH^{KO}-I/R, LBH^{KO}-Lv5NC-I/R and LBH^{KO}-LBH-I/R mice.

(D) Relative iron and MDA concentrations measured in the ischemic heart tissue of LBH^{WT}-Sham, LBH^{KO}-I/R, LBH^{KO}-Lv5NC-I/R and LBH^{KO}-LBH-I/R mice (Brown-Forsythe ANOVA test, *** = $p < 0.001$ vs. LBH^{WT}-Sham; ^^^ = $p < 0.001$ vs. LBH^{KO}-Lv5NC-I/R. Error bars are mean ± SD).

(E) Protein expression of LBH, p-P38, P38, *p*-CRYAB, CRYAB, p-53, NRF2 and GPX4 in the ischemic heart tissue of lentivirus-transfected LBH^{WT} mice/LBH^{KO} mice (Brown-Forsythe ANOVA test, ** = $p < 0.01$ and *** = $p < 0.001$ vs. LBH^{WT}-Sham; ^^ = $p < 0.01$ and ^^^ = $p < 0.001$ vs. LBH^{KO}-Lv5NC-I/R. Error bars are mean ± SD).

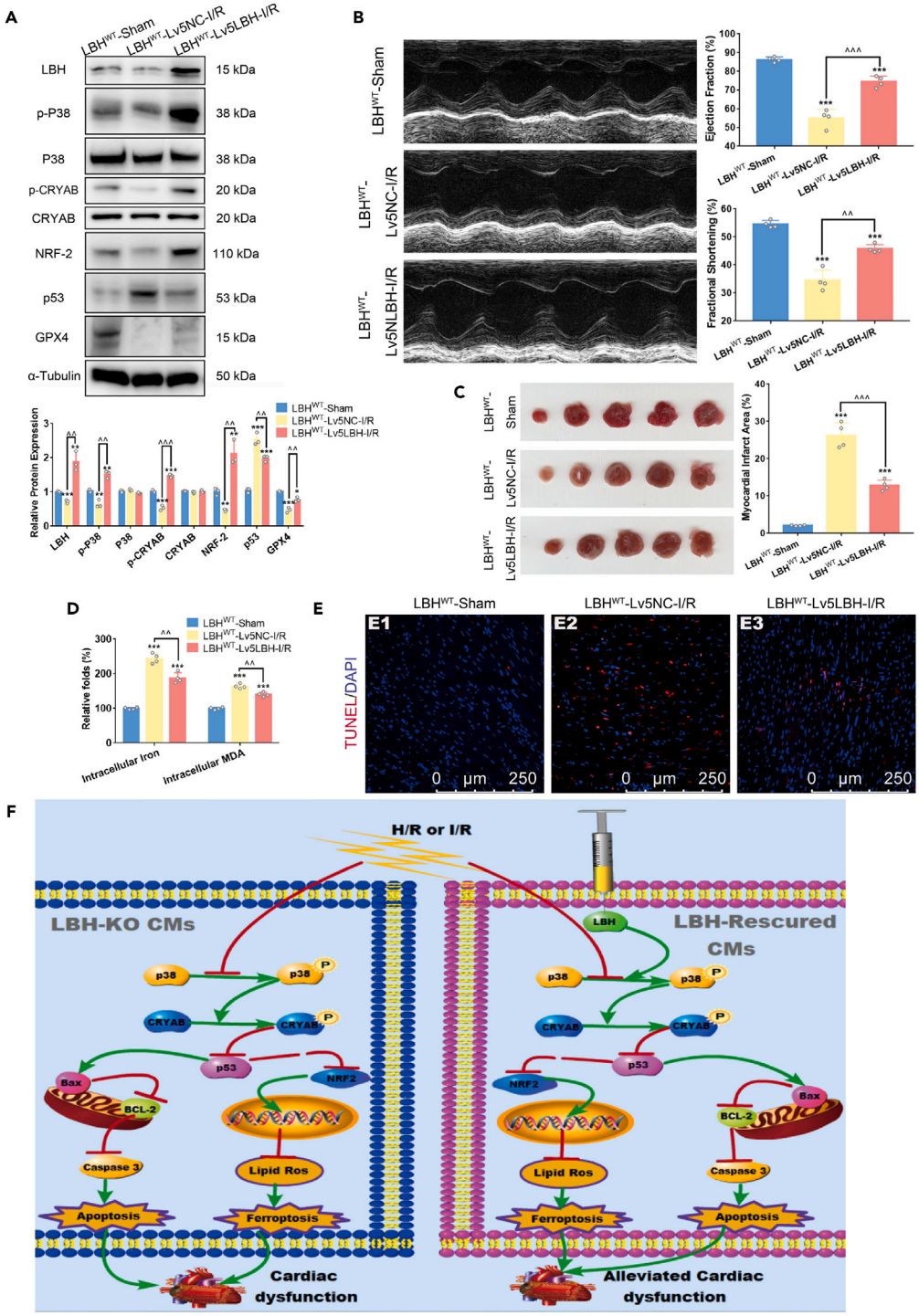

Figure 11. LBH overexpression in LBH^{WT} mice before ischemia-reperfusion treatment enhances cardiac protection against the following apoptosis, ferroptosis, and cardiac dysfunction

(A) Protein expression of LBH, p-P38, P38, *p*-CRYAB, CRYAB, p-53, NRF2 and GPX4 in the ischemic heart tissue of lentivirus-transfected LBH^{WT} mice (Brown-Forsythe ANOVA test, * = $p < 0.05$, ** = $p < 0.01$, *** = $p < 0.001$ vs. LBH^{WT}-Sham; ^ = $p < 0.05$, ^^ = $p < 0.01$, ^^^ = $p < 0.001$ vs. LBH^{WT}-Lv5NC-I/R. Error bars are mean ± SD).

(B) Representative echocardiograms of LBH^{WT}-Sham, LBH^{WT}-Lv5NC-I/R and LBH^{WT}-LBH-I/R mice and the corresponding statistical analysis of cardiac EFs and FSs (Brown-Forsythe ANOVA test, *** = $p < 0.001$ vs. LBH^{WT}-Sham; ^^^ = $p < 0.001$ vs. LBH^{WT}-Lv5NC-I/R. Error bars are mean ± SD).

Figure 11. *Continued*

(C) Representative TTC staining of heart cross-sections of LBH^{WT}-Sham, LBH^{WT}-Lv5NC-I/R and LBH^{WT}-LBH-I/R mice and the corresponding statistical analysis of myocardial infarct areas indicated by the staining (Brown-Forsythe ANOVA test, * = $p < 0.05$, ** = $p < 0.01$ and *** = $p < 0.001$ vs. LBH^{WT}-Sham; ^^ = $p < 0.01$ ^^^ = $p < 0.001$ vs. LBH^{WT}-Lv5NC-I/R. Error bars are mean ± SD).

(D) Relative iron and MDA concentrations measured in ischemic heart tissue of LBH^{WT}-Sham, LBH^{WT}-Lv5NC-I/R and LBH^{WT}-LBH-I/R mice (Brown-Forsythe ANOVA test, *** = $p < 0.001$ vs. LBH^{WT}-Sham; ^^ = $p < 0.01$ vs. LBH^{WT}-Lv5NC-I/R. Error bars are mean ± SD).

(E) Representative TUNEL staining of heart cross-sections of LBH^{WT}-Sham, LBH^{WT}-Lv5NC-I/R and LBH^{WT}-LBH-I/R mice.

(F) Schematic summary of the LBH-mediated p38-CRYAB signaling responsible for simultaneously modulating mitochondrial apoptosis and ferroptosis in cardiomyocytes during hypoxia-reoxygenation.

- ○ Dual-luciferase reporter assay
- ● QUANTIFICATION AND STATISTICAL ANALYSIS

SUPPLEMENTAL INFORMATION

Supplemental information can be found online at https://doi.org/10.1016/j.isci.2024.109510.

ACKNOWLEDGMENTS

This work was funded by the National Natural Science Foundation of China (No. 82070247).

AUTHOR CONTRIBUTIONS

A.W. and C. L. designed the study. A.W., C.Z., X.S., and T.S. performed the experiments. W.Y. and M.T. participate in the animal procedures. A.W. and C.Z. analyzed and visualized the experimental data. A.W. wrote the original draft. C.L. and P.Y. supervised the study and reviewed the article for submission. A.W., C.Z., and H.H. completed the revision.

DECLARATION OF INTERESTS

The authors have declared that no competing interests exists.

Received: September 10, 2023
Revised: December 29, 2023
Accepted: March 13, 2024
Published: March 15, 2024

REFERENCES

1. Li, Y.Q., Gao, Y., and Li, G.P. (2022). Preclinical multi-target strategies for myocardial ischemia-reperfusion injury. Front Cardiovasc Med *9*, 967115. https://doi.org/10.3389/fcvm.2022.967115.
2. Ibáñez, B., Heusch, G., Ovize, M., and Van de Werf, F. (2015). Evolving therapies for myocardial ischemia/reperfusion injury. J. Am. Coll. Cardiol. *65*, 1454–1471. https://doi.org/10.1016/j.jacc.2015.02.032.
3. Freiberg, R.A., Krieg, A.J., Giaccia, A.J., and Hammond, E.M. (2006). Checking in on hypoxia/reoxygenation. Cell Cycle *5*, 1304–1307. https://doi.org/10.4161/cc.5.12.2811.
4. Kloner, R.A. (2013). Current state of clinical translation of cardioprotective agents for acute myocardial infarction. Circ. Res. *113*, 451–463. https://doi.org/10.1161/CIRCRESAHA.112.300627.
5. Schirone, L., Forte, M., D'Ambrosio, L., Valenti, V., Vecchio, D., Schiavon, S., Spinosa, G., Sarto, G., Petrozza, V., Frati, G., and Sciarretta, S. (2022). An Overview of the Molecular Mechanisms Associated with Myocardial Ischemic Injury: State of the Art and Translational Perspectives. Cells *11*, 1165. https://doi.org/10.3390/cells11071165.
6. Hausenloy, D.J., and Yellon, D.M. (2013). Myocardial ischemia-reperfusion injury: a neglected therapeutic target. J. Clin. Invest. *123*, 92–100. https://doi.org/10.1172/JCI62874.
7. Braunwald, E., and Kloner, R.A. (1985). Myocardial reperfusion: a double-edged sword? J. Clin. Invest. *76*, 1713–1719. https://doi.org/10.1172/JCI112160.
8. Ferreira, R. (2010). The reduction of infarct size–forty years of research. Rev. Port. Cardiol. *29*, 1037–1053.
9. Heusch, G., and Gersh, B.J. (2017). The pathophysiology of acute myocardial infarction and strategies of protection beyond reperfusion: a continual challenge. Eur. Heart J. *38*, 774–784. https://doi.org/10.1093/eurheartj/ehw224.
10. Briegel, K.J., and Joyner, A.L. (2001). Identification and characterization of Lbh, a novel conserved nuclear protein expressed during early limb and heart development. Dev. Biol. *233*, 291–304. https://doi.org/10.1006/dbio.2001.0225.
11. Briegel, K.J., Baldwin, H.S., Epstein, J.A., and Joyner, A.L. (2005). Congenital heart disease reminiscent of partial trisomy 2p syndrome in mice transgenic for the transcription factor LBH. Development *132*, 3305–3316. https://doi.org/10.1242/dev.01887.
12. wu, A., Zhang, L., Chen, J., Li, H., Yang, P., Chen, M., and Liu, Q. (2021). Limb-bud and Heart (LBH) mediates proliferation, fibroblast-to-myofibroblast transition and EMT- like processes in cardiac fibroblasts. Mol. Cell. Biochem. *476*, 2685–2701. https://doi.org/10.1007/s11010.
13. Xu, Y., Wu, A., Chen, J., Song, X., Chen, M., and Liu, Q. (2022). Limb-Bud and Heart (LBH) upregulation in cardiomyocytes under hypoxia promotes the activation of cardiac fibroblasts via exosome secretion. Mediat. Inflamm. *2022*, 8939449. https://doi.org/10.1155/2022/8939449.
14. Del Re, D.P., Amgalan, D., Linkermann, A., Liu, Q., and Kitsis, R.N. (2019). Fundamental Mechanisms of Regulated Cell Death and Implications for Heart Disease. Physiol. Rev. *99*, 1765–1817. https://doi.org/10.1152/physrev.00022.2018.
15. Indran, I.R., Tufo, G., Pervaiz, S., and Brenner, C. (2011). Recent advances in apoptosis, mitochondria and drug resistance in cancer cells. Biochim. Biophys. Acta *1807*, 735–745. https://doi.org/10.1016/j.bbabio.2011.03.010.
16. Pradelli, L.A., Bénéteau, M., and Ricci, J.E. (2010). Mitochondrial control of caspase-dependent and -independent cell death. Cell. Mol. Life Sci. *67*, 1589–1597. https://doi.org/10.1007/s00018-010-0285-y.
17. Dixon, S.J., Lemberg, K.M., Lamprecht, M.R., Skouta, R., Zaitsev, E.M., Gleason, C.E., Patel, D.N., Bauer, A.J., Cantley, A.M., Yang, W.S., et al. (2012). Ferroptosis: an iron-dependent form of nonapoptotic cell death. Cell *149*,

1060–1072. https://doi.org/10.1016/j.cell.2012.03.042.
18. Yan, H.F., Zou, T., Tuo, Q.Z., Xu, S., Li, H., Belaidi, A.A., and Lei, P. (2021). Ferroptosis: mechanisms and links with diseases. Signal Transduct. Targeted Ther. *6*, 49. https://doi.org/10.1038/s41392-020-00428-9.
19. Wu, X., Li, Y., Zhang, S., and Zhou, X. (2021). Ferroptosis as a novel therapeutic target for cardiovascular disease. Theranostics *11*, 3052–3059. https://doi.org/10.7150/thno.54113.
20. Li, J., Cao, F., Yin, H.L., Huang, Z.J., Lin, Z.T., Mao, N., Sun, B., and Wang, G. (2020). Ferroptosis: past, present and future. Cell Death Dis. *11*, 88. https://doi.org/10.1038/s41419-020-2298-2.
21. Zhu, S., Zhang, Q., Sun, X., Zeh, H.J., 3rd, Lotze, M.T., Kang, R., and Tang, D. (2017). HSPA5 Regulates Ferroptotic Cell Death in Cancer Cells. Cancer Res. *77*, 2064–2077. https://doi.org/10.1158/0008-5472.CAN-16-1979.
22. Kamradt, M.C., Chen, F., and Cryns, V.L. (2001). The small heat shock protein alpha B-crystallin negatively regulates cytochrome c- and caspase-8-dependent activation of caspase-3 by inhibiting its autoproteolytic maturation. J. Biol. Chem. *276*, 16059–16063. https://doi.org/10.1074/jbc.C100107200.
23. Mao, Y.W., Liu, J.P., Xiang, H., and Li, D.W.C. (2004). Human alphaA- and alphaB-crystallins bind to Bax and Bcl-X(S) to sequester their translocation during staurosporine-induced apoptosis. Cell Death Differ. *11*, 512–526. https://doi.org/10.1038/sj.cdd.4401384.
24. Peng, Y., Yu, H., Zhang, Y., Qu, F., Tang, Z., Qu, C., Tian, J., Zong, B., Wang, Y., Ren, H., and Liu, S. (2021). A ferroptosis-associated gene signature for the prediction of prognosis and therapeutic response in luminal-type breast carcinoma. Sci. Rep. *11*, 17610. https://doi.org/10.1038/s41598-021-97102-z.
25. Yan, Y., Cai, J., Huang, Z., Cao, X., Tang, P., Wang, Z., Zhang, F., Xia, S., and Shen, B. (2021). A Novel Ferroptosis-Related Prognostic Signature Reveals Macrophage Infiltration and EMT Status in Bladder Cancer. Front. Cell Dev. Biol. *9*, 712230. https://doi.org/10.3389/fcell.2021.712230.
26. Wang, X., Zhang, G., Dasgupta, S., Niewold, E.L., Li, C., Li, Q., Luo, X., Tan, L., Ferdous, A., Lorenzi, P.L., et al. (2022). ATF4 Protects the Heart from Failure by Antagonizing Oxidative Stress. Circ. Res. *131*, 91–105. https://doi.org/10.1161/CIRCRESAHA.122.321050.
27. Fang, X., Cai, Z., Wang, H., Han, D., Cheng, Q., Zhang, P., Gao, F., Yu, Y., Song, Z., Wu, Q., et al. (2020). Loss of Cardiac Ferritin H Facilitates Cardiomyopathy via Slc7a11-Mediated Ferroptosis. Circ. Res. *127*, 486–501. https://doi.org/10.1161/CIRCRESAHA.120.316509.
28. Fuchs, Y., and Steller, H. (2011). Programmed cell death in animal development and disease. Cell *147*, 742–758. https://doi.org/10.1016/j.cell.2011.10.033.
29. Wu, A., Luo, N., Xu, Y., Du, N., Li, L., and Liu, Q. (2022). Exosomal LBH inhibits epithelial-mesenchymal transition and angiogenesis in nasopharyngeal carcinoma via downregulating VEGFA signaling. Int. J. Biol. Sci. *18*, 242–260. https://doi.org/10.7150/ijbs.66506.
30. Boelens, W.C. (2014). Cell biological roles of αB-crystallin. Prog. Biophys. Mol. Biol. *115*, 3–10. https://doi.org/10.1016/j. pbiomolbio.2014.02.005.
31. Muraleva, N.A., Kolosova, N.G., and Stefanova, N.A. (2019). p38 MAPK-dependent alphaB-crystallin phosphorylation in Alzheimer's disease-like pathology in OXYS rats. Exp. Gerontol. *119*, 45–52. https://doi.org/10.1016/j. exger.2019.01.017.
32. Nishizawa, H., Matsumoto, M., Shindo, T., Saigusa, D., Kato, H., Suzuki, K., Sato, M., Ishii, Y., Shimokawa, H., and Igarashi, K. (2020). Ferroptosis is controlled by the coordinated transcriptional regulation of glutathione and labile iron metabolism by the transcription factor BACH1. J. Biol. Chem. *295*, 69–82. https://doi.org/10.1074/jbc. RA119.009548.
33. Friedmann Angeli, J.P., Schneider, M., Proneth, B., Tyurina, Y.Y., Tyurin, V.A., Hammond, V.J., Herbach, N., Aichler, M., Walch, A., Eggenhofer, E., et al. (2014). Inactivation of the ferroptosis regulator Gpx4 triggers acute renal failure in mice. Nat. Cell Biol. *16*, 1180–1191. https://doi.org/10.1038/ncb3064.
34. Xie, Y., Hou, W., Song, X., Yu, Y., Huang, J., Sun, X., Kang, R., and Tang, D. (2016). Ferroptosis: process and function. Cell Death Differ. *23*, 369–379. https://doi.org/10.1038/cdd.2015.158.
35. Deng, Y., Li, Y., Fan, X., Yuan, W., Xie, H., Mo, X., Yan, Y., Zhou, J., Wang, Y., Ye, X., et al. (2010). Synergistic efficacy of LBH and alphaB-crystallin through inhibiting transcriptional activities of p53 and p21. BMB Rep. *43*, 432–437. https://doi.org/10.5483/bmbrep.2010.43.6.432.
36. Liu, S., Li, J., Tao, Y., and Xiao, X. (2007). Small heat shock protein alphaB-crystallin binds to p53 to sequester its translocation to mitochondria during hydrogen peroxide-induced apoptosis. Biochem. Biophys. Res. Commun. *354*, 109–114. https://doi.org/10.1016/j.bbrc.2006.12.152.
37. Yuan, H., Pratte, J., and Giardina, C. (2021). Ferroptosis and its potential as a therapeutic target. Biochem. Pharmacol. *186*, 114486. https://doi.org/10.1016/j.bcp.2021.114486.
38. Muraleva, N.A., Devyatkin, V.A., and Kolosova, N.G. (2017). Phosphorylation of αB-crystallin in the myocardium: Analysis of relations with aging and cardiomyopathy. Exp. Gerontol. *95*, 26–33. https://doi.org/10.1016/j.exger.2017.05.009.
39. Wu, A., Zhang, L., Luo, N., Zhang, L., Li, L., and Liu, Q. (2021). Limb-bud and heart (LBH) inhibits cellular migration, invasion and epithelial-mesenchymal transition in nasopharyngeal carcinoma via downregulating αB-crystallin expression. Cell. Signal. *85*, 110045. https://doi.org/10.1016/j.cellsig.2021.110045.
40. Chen, D., Tavana, O., and Gu, W. (2018). ARF-NRF2: A new checkpoint for oxidative stress responses? Mol. Cell. Oncol. *5*, e1432256. https://doi.org/10.1080/23723556.2018.1432256.
41. Jenkins, T., and Gouge, J. (2021). Nrf2 in Cancer, Detoxifying Enzymes and Cell Death Programs. Antioxidants *10*, 1030. https://doi.org/10.3390/antiox10071030.
42. Qiu, Y.B., Wan, B.B., Liu, G., Wu, Y.X., Chen, D., Lu, M.D., Chen, J.L., Yu, R.Q., Chen, D.Z., and Pang, Q.F. (2020). Nrf2 protects against seawater drowning-induced acute lung injury via inhibiting ferroptosis. Respir. Res. *21*, 232. https://doi.org/10.1186/s12931-020-01500-2.
43. Sun, X., Ou, Z., Chen, R., Niu, X., Chen, D., Kang, R., and Tang, D. (2016). Activation of the p62-Keap1-NRF2 pathway protects against ferroptosis in hepatocellular carcinoma cells. Hepatology *63*, 173–184. https://doi.org/10.1002/hep.28251.
44. Fan, Z., Wirth, A.-K., Chen, D., Wruck, C.J., Rauh, M., Buchfelder, M., and Savaskan, N. (2017). Nrf2-Keap1 pathway promotes cell proliferation and diminishes ferroptosis. Oncogenesis *6*, e371. https://doi.org/10.1038/oncsis.2017.65.
45. Xu, S., Wu, B., Zhong, B., Lin, L., Ding, Y., Jin, X., Huang, Z., Lin, M., Wu, H., and Xu, D. (2021). Naringenin alleviates myocardial ischemia/reperfusion injury by regulating the nuclear factor-erythroid factor 2-related factor 2 (Nrf2)/System xc-/glutathione peroxidase 4 (GPX4) axis to inhibit ferroptosis. Bioengineered *12*, 10924–10934. https://doi.org/10.1080/21655979.2021.1995994.
46. Fittipaldi, S., Mercatelli, N., Dimauro, I., Jackson, M.J., Paronetto, M.P., and Caporossi, D. (2015). Alpha B-crystallin induction in skeletal muscle cells under redox imbalance is mediated by a JNK-dependent regulatory mechanism. Free Radic. Biol. Med. *86*, 331–342. https://doi.org/10.1016/j.freeradbiomed.2015.05.035.
47. Mitra, A., Ray, A., Datta, R., Sengupta, S., and Sarkar, S. (2014). Cardioprotective role of P38 MAPK during myocardial infarction via parallel activation of α-crystallin B and Nrf2. J. Cell. Physiol. *229*, 1272–1282. https://doi.org/10.1002/jcp.24565.
48. Watanabe, G., Kato, S., Nakata, H., Ishida, T., Ohuchi, N., and Ishioka, C. (2009). alphaB-crystallin: a novel p53-target gene required for p53-dependent apoptosis. Cancer Sci. *100*, 2368–2375. https://doi.org/10.1111/j.1349-7006. 2009.01316.x.
49. Evans, J.R., Bosman, J.D., Brown-Endres, L., Yehiely, F., and Cryns, V.L. (2010). Induction of the small heat shock protein alphaB-crystallin by genotoxic stress is mediated by p53 and p73. Breast Cancer Res. Treat. *122*, 159–168. https://doi.org/10.1007/s10549-009-0542-7.
50. Liu, S., Yan, B., Lai, W., Chen, L., Xiao, D., Xi, S., Jiang, Y., Dong, X., An, J., Chen, X., et al. (2014). As a novel p53 direct target, bidirectional gene HspB2/αB-crystallin regulates the ROS level and Warburg effect. Biochim. Biophys. Acta *1839*, 592–603. https://doi.org/10.1016/j.bbagrm.2014.05.017.
51. Chen, Q., Thompson, J., Hu, Y., and Lesnefsky, E.J. (2020). Cardiomyocyte specific deletion of p53 decreases cell injury during ischemia-reperfusion: Role of Mitochondria. Free Radic. Biol. Med. *158*, 162–170. https://doi.org/10.1016/j.freeradbiomed.2020.06.006.
52. Liu, Y., and Gu, W. (2022). p53 in ferroptosis regulation: the new weapon for the old guardian. Cell Death Differ. *29*, 895–910. https://doi.org/10.1038/s41418-022-00943-y.
53. Liu, J., Zhang, C., Wang, J., Hu, W., and Feng, Z. (2020). The Regulation of Ferroptosis by Tumor Suppressor p53 and its Pathway. Int. J. Mol. Sci. *21*, 8387. https://doi.org/10.3390/ijms21218387.
54. Jiang, L., Kon, N., Li, T., Wang, S.J., Su, T., Hibshoosh, H., Baer, R., and Gu, W. (2015). Ferroptosis as a p53-mediated activity during tumour suppression. Nature *520*, 57–62. https://doi.org/10.1038/nature14344.
55. Hong, T., Lei, G., Chen, X., Li, H., Zhang, X., Wu, N., Zhao, Y., Zhang, Y., and Wang, J. (2021). PARP inhibition promotes ferroptosis via repressing SLC7A11 and synergizes with ferroptosis inducers in BRCA-proficient

ovarian cancer. Redox Biol. *42*, 101928. https://doi.org/10.1016/j.redox.2021.101928.
56. Ma, S., Sun, L., Wu, W., Wu, J., Sun, Z., and Ren, J. (2020). USP22 Protects Against Myocardial Ischemia-Reperfusion Injury via the SIRT1-p53/SLC7A11-Dependent Inhibition of Ferroptosis-Induced Cardiomyocyte Death. Front. Physiol. *11*, 551318. https://doi.org/10.3389/fphys.2020.551318.
57. Chen, W., Jiang, T., Wang, H., Tao, S., Lau, A., Fang, D., and Zhang, D.D. (2012). Does Nrf2 contribute to p53-mediated control of cell survival and death? Antioxidants Redox Signal. *17*, 1670–1675. https://doi.org/10.1089/ars.2012.4674.
58. Ju, J., Song, Y.N., and Wang, K. (2021). Mechanism of Ferroptosis: A Potential Target for Cardiovascular Diseases Treatment. Aging Dis. *12*, 261–276. https://doi.org/10.14336/AD.2020.0323.
59. Yu, Y., Yan, Y., Niu, F., Wang, Y., Chen, X., Su, G., Liu, Y., Zhao, X., Qian, L., Liu, P., and Xiong, Y. (2021). Ferroptosis: a cell death connecting oxidative stress, inflammation and cardiovascular diseases. Cell Death Dis. *7*, 193. https://doi.org/10.1038/s41420-021-00579-w.
60. Chen, Y., Fan, H., Wang, S., Tang, G., Zhai, C., and Shen, L. (2021). Ferroptosis: A Novel Therapeutic Target for Ischemia-Reperfusion Injury. Front. Cell Dev. Biol. *9*, 688605. https://doi.org/10.3389/fcell.2021.688605.
61. Yang, Y., Zhang, Y., Yang, J., Zhang, M., Tian, T., Jiang, Y., Liu, X., Xue, G., Li, X., Zhang, X., et al. (2023). Interdependent Nuclear Co-Trafficking of ASPP1 and p53 Aggravates Cardiac Ischemia/Reperfusion Injury. Circ. Res. *132*, 208–222. https://doi.org/10.1161/CIRCRESAHA.122. 321153.
62. Dong, Y., Chen, H., Gao, J., Liu, Y., Li, J., and Wang, J. (2019). Molecular machinery and interplay of apoptosis and autophagy in coronary heart disease. J. Mol. Cell. Cardiol. *136*, 27–41. https://doi.org/10.1016/j.yjmcc.2019.09.001.
63. Tang, L.J., Zhou, Y.J., Xiong, X.M., Li, N.S., Zhang, J.J., Luo, X.J., and Peng, J. (2021). Ubiquitin-specific protease 7 promotes ferroptosis via activation of the p53/TfR1 pathway in the rat hearts after ischemia/reperfusion. Free Radic. Biol. Med. *162*, 339–352. https://doi.org/10.1016/j.freeradbiomed.2020.10.307.
64. Celie, P.H., Parret, A.H., and Perrakis, A. (2016). Recombinant cloning strategies for protein expression. Curr. Opin. Struct. Biol. *38*, 145–154. https://doi.org/10.1016/j.sbi.2016.06.010.
65. Wingfield, P.T. (2015). Overview of the purification of recombinant proteins. Curr. Protoc. Protein Sci. *80*, 6.1.1–6.1.35. https://doi.org/10.1002/0471140864.ps0601s80.
66. Yue, P., Zhang, Y., Liu, L., Zhou, K., Xia, S., Peng, M., Yan, H., Tang, X., Chen, Z., Zhang, D., et al. (2022). Yap1 modulates cardiomyocyte hypertrophy via impaired mitochondrial biogenesis in response to chronic mechanical stress overload. Theranostics *12*, 7009–7031. https://doi.org/10.7150/thno.74563.
67. Liu, Z., Liu, X., Liu, L., Wang, Y., Zheng, J., Li, L., Li, S., Zhang, H., Ni, J., Ma, C., et al. (2023). SUMO1 regulates post-infarct cardiac repair based on cellular heterogeneity. J. Pharm. Anal. *13*, 170–186. https://doi.org/10.1016/j.jpha. 2022.11.010.
68. Yet, S.F., Tian, R., Layne, M.D., Wang, Z.Y., Maemura, K., Solovyeva, M., Ith, B., Melo, L.G., Zhang, L., Ingwall, J.S., et al. (2001). Cardiac-specific expression of heme oxygenase-1 protects against ischemia and reperfusion injury in transgenic mice. Circ. Res. *89*, 168–173. https://doi.org/10.1161/hh1401.093314.
69. Sadoshima, J., and Izumo, S. (1993). Molecular characterization of angiotensin II–induced hypertrophy of cardiac myocytes and hyperplasia of cardiac fibroblasts: Critical role of the AT1 receptor subtype. Circ. Res. *73*, 413–423. https://doi.org/10.1161/01.res.73.3.413.
70. Davidson, M.M., Nesti, C., Palenzuela, L., Walker, W.F., Hernandez, E., Protas, L., Hirano, M., and Isaac, N.D. (2005). Novel cell lines derived from adult human ventricular cardiomyocytes. J. Mol. Cell. Cardiol. *39*, 133–147. https://doi.org/10.1016/j.yjmcc.2005.03.003.
71. Si, L., Bai, H., Rodas, M., Cao, W., Oh, C.Y., Jiang, A., Moller, R., Hoagland, D., Oishi, K., Horiuchi, S., et al. (2021). A human-airway-on-a-chip for the rapid identification of candidate antiviral therapeutics and prophylactics. Nat. Biomed. Eng. *5*, 815–829. https://doi.org/10.1038/s41551-021-00718-9.
72. Liu, P., Feng, Y., Li, H., Chen, X., Wang, G., Xu, S., Li, Y., and Zhao, L. (2020). Ferrostatin-1 alleviates lipopolysaccharide-induced acute lung injury via inhibiting ferroptosis. Cell. Mol. Biol. Lett. *25*, 10. https://doi.org/10.1186/s11658-020-00205-0.
73. Ran, G., Fang, W., Zhang, L., Peng, Y., Wu, A., Li, J., Ding, X., Zeng, S., and He, Y. (2021). Polypeptides IGF-1C and P24 synergistically promote osteogenic differentiation of bone marrow mesenchymal stem cells in vitro through the p38 and JNK signaling pathways. Int. J. Biochem. Cell Biol. *141*, 106091. https://doi.org/10.1016/j.biocel. 2021.106091.
74. Schneider, C.A., Rasband, W.S., and Eliceiri, K.W. (2012). NIH Image to ImageJ: 25 years of image analysis. Nat. Methods *9*, 671–675. https://doi.org/10.1038/nmeth.2089.
75. Van Rheenen, J., Langeslag, M., and Jalink, K. (2004). Correcting confocal acquisition to optimize imaging of Fluorescence Resonance Energy Transfer by sensitized emission. Biophys. J. *86*, 2517–2529. https://doi.org/10.1016/S0006-3495(04)74307-6.
76. Tuck, S.P., and Crawford, L. (1989). Characterization of the human p53 gene promoter. Mol. Cell Biol. *9*, 2163–2172. https://doi.org/10.1128/mcb.9.5.2163-2172.1989.

STAR★METHODS

KEY RESOURCES TABLE

REAGENT or RESOURCE	SOURCE	IDENTIFIER
Antibodies		
Rabbit anti-LBH	Abcam	Cat#: ab173737; RRID: AB_2313773
Rabbit anti-LBH	Abcam	Cat#: ab122223; RRID: AB_11127118
Rabbit anti-CRYAB	Proteintech	Cat#: 15808-1-AP; RRID: AB_2292175
Rabbit anti-CRYAB	Abcam	Cat#: ab76467; RRID: AB_1523120
Rabbit anti-phospho-CRYAB (Ser59)	Abcam	Cat#: ab5577; RRID: AB_304959
Rabbit anti-GPX4	Cell Signaling Technology	Cat#: 59735; RRID: AB_2940796
Rabbit anti-NRF2	Proteintech	Cat#: 16396-1-AP; RRID: AB_2782956
Rabbit anti-KEAP1	Proteintech	Cat#: 10503-2-AP; RRID: AB_2132625
Rabbit anti-Lamin B1	Proteintech	Cat#: 12987-1-AP; RRID: AB_2136290
Mouse anti-p53	Abcam	Cat#: ab26; RRID: AB_303198
Rabbit anti-p53	Proteintech	Cat#: 10442-1-AP; RRID: AB_2206609
Rabbit anti-cleaved Caspase 3 (Asp175)	Cell Signaling Technology	Cat#: 9661; RRID: AB_2341188
Rabbit anti-Bax	Sigma-Aldrich	Cat#: B3428; RRID: AB_258547
Rabbit anti-BCL2	Sigma-Aldrich	Cat#: SAB4500003; RRID: AB_10743656
Rabbit anti-HIF-1α	Thermo Fisher Scientific	Cat#: PA1-16601; RRID: AB_2117128
Rabbit anti-p38	Cell Signaling Technology	Cat#: 9212; RRID: AB_330713
Rabbit anti-phospho-p38 (Thr180/Tyr182)	Cell Signaling Technology	Cat#: 9211; RRID: AB_331641
Rabbit anti-GAPDH	Bioworld Technology	Cat#: AP0063; RRID: AB_2651132
Rabbit anti-α-Tubulin	Proteintech	Cat#: 66031-1-Ig, RRID: AB_11042766
Mouse anti-β-Actin	Bioworld Technology	Cat#: BS6007M; RRID: AB_2904238
Rabbit anti-Cardiac myosin	Abcam	Cat#: ab46936; RRID: AB_1523211
Rabbit anti-CTnT	Abcam	Cat#: EPR20266; RRID: N/A
Rabbit anti-α-Actinin	Abcam	Cat#: ab68194; RRID: AB_3064857
Rabbit anti-GSDMD	Novus	Cat#: NBP2-33422; RRID: AB_2687913
Rabbit anti-phospho-MLKL (Ser345)	Novus	Cat#: NBP2-66953; RRID: AB_2927747
Rabbit anti-LC3	Abcam	Cat#: ab192890; RRID: AB_2827794
Goat anti-rabbit IgG-HRP	Cell Signaling Technology	Cat#: 7074; RRID: AB_2099233
Horse anti-mouse IgG-HRP	Cell Signaling Technology	Cat#: 7076; RRID: AB_330924
Goat anti-mouse-Alexa Fluor 488	Thermo Fisher Scientific	Cat#: A-11001; RRID: AB_2534069
Donkey anti-rabbit-Alexa Fluor Plus 488	Thermo Fisher Scientific	Cat#: A-21206; RRID: AB_2535792
Donkey anti-rabbit-Alexa Fluor Plus 555	Thermo Fisher Scientific	Cat#: A-31572; RRID: AB_162543
Goat anti-mouse-Alexa Fluor 790	Thermo Fisher Scientific	Cat#: A11357; RRID: AB_2534140
Goat anti-rabbit-Alexa Fluor 680	Thermo Fisher Scientific	Cat#: A32734; RRID: AB_2633283
anti-mouse IgG for IP, AlpsdAbs@VHH (HRP)	AlpVHHs	Cat#: 001-100-005; RRID: AB_2313773
anti-rabbit IgG for IP, AlpsdAbs@VHH (HRP)	AlpVHHs	Cat#: 025-100-005; RRID: AB_2313773
Bacterial and virus strains		
Lv3-NC-eGFP	Genepharma	Cat#: E23BZ; Lot#: 15-0798Z
Lv5-NC-eGFP	Genepharma	Cat#: E13HZ; Lot#: 22-4739Z
Lv3-shLBH-eGFP	Genepharma	Cat#: T2085; Lot#: 15-0797Z
Lv3-human LBH-eGFP (NM_030915.4)	Genepharma	Cat#: Y1658; Lot#: 16-0041Z
Lv5-rat LBH-eGFP (NM_001129880)	Genepharma	Cat#: Y2263; Lot#: 22-4738Z

(*Continued on next page*)

Continued

REAGENT or RESOURCE	SOURCE	IDENTIFIER
Chemicals, peptides, and recombinant proteins		
PBS	Gibco	Cat#: 10010023
Penicillin-streptomycin	Gibco	Cat#: 15140122
Isoflurane	RWD	Cat#: R510-22
0.25% EDTA-trypsin	Gibco	Cat#: 27250018
collagenase II	Beyotime	Cat#: ST2303
DMEM	Gibco	Cat#: 11965092
DMEM/F12	Gibco	Cat#: 11320033
glucose-free, serum-free DMEM	Gibco	Cat#: 11966025
FBS	Gibco	Cat#: 10099141
BrdU	Beyotime	Cat#: ST1056
TRIzol® reagent	Thermo Fisher Scientific	Cat#: 15596026
Ralimetinib	Selleck	Cat#: LY228820; CAS: 862507-23-1
Erastin	MCE	Cat#: HY-15763; CAS: 571203-78-6
Chloroquine diphosphate	Abcam	Cat#: ab142116; CAS: 50-63-5
Ferrostatin	MCE	Cat#: HY-100579; CAS: 347174-05-4
Tetrazolium Red (2,3,5-Triphenyltetrazolium chloride; TTC)	MCE	Cat#: HY-D0714; CAS: 298-96-4
Lipofectamine™ 3000 reagent	Thermo Fisher Scientific	Cat#: L3000015
RIPA lysis buffer	Thermo Fisher Scientific	Cat#: 89901
DAPI	Thermo Fisher Scientific	Cat#: D21490
Restore™ Membrane stripping buffer	Thermo Fisher Scientific	Cat#: 21059
Critical commercial assays		
TUNEL assay kit	Beyotime	Cat#: C1090
Annexin V/7-AAD staining kit	Thermo Fisher Scientific	Cat#: 88-8102-72
Total iron colorimetric assay kit	Leagene	Cat#: E1042
Malondialdehyde colorimetric assay kit	Beyotime	Cat#: S0131
FerroOrange™ staining kit	Dojindo	Cat#: F374
PrimeScript™ RT reagent kit	Takara	Cat#: RR037B
SYBR® Premix Ex Taq TM kit	Takara	Cat#: RR003A
NE-PER™ kit	Thermo Fisher Scientific	Cat#: 78833
Protein A/G magnetic beads	Bimake	Cat#: B23202
ProLong™ mounting medium	Thermo Fisher Scientific	Cat#: P36930
Dual-luciferase reporter assay kit	Yeason	Cat#: 11402ES60
real-time cell analyzer system	ACEA Biosciences	Cat#: RTCA-DP
CCK-8 assay kit	Dojindo	Cat#: CK04
Experimental models: Cell lines		
Rat:H9C2	ATCC	Cat#: CRL-1446
Human:AC16	ATCC	Cat#: CRL-3568
Mouse: HL1	Sigma-Aldrich	Cat#: SCC065
Experimental models: Organisms/strains		
Mouse: C57BL/6 mice	Experimental Animal Center of Southern Medical University	N/A
Mouse: conventional LBH^{KO} C57BL/6 mice	Cyagen	contract ID: KOAI200813MG1

(*Continued on next page*)

Continued

REAGENT or RESOURCE	SOURCE	IDENTIFIER
Oligonucleotides		
Primers for rat LBH, see Table S1	This paper	N/A
Primers for rat NRF2, see Table S1	This paper	N/A
Primers for rat β-Actin, see Table S1	This paper	N/A
Primers for mouse LBH, see Table S1	This paper	N/A
Primers for mouse p53, see Table S1	This paper	N/A
Primers for mouse NRF2, see Table S1	This paper	N/A
Primers for mouse β-Actin, see Table S1	This paper	N/A
rowheadRecombinant DNA		
Plasmid: pCDH-CMV-gfp-eGFP-EF1-Puro	Kidan Bio	Lot#: JD-M190521089-1
Plasmid: pLV-CMV-mCherry-6His-IRES-Bla	Kidan Bio	Lot#: JD-M190521089-2
Plasmid: pCDH-CMV-TP53-gfp-eGFP-EF1-Puro (NM_00546)	Kidan Bio	Lot#: JD-M06082089-1
Plasmid: pLV-CMV-CRYAB-mCherry-6His-IRES-Bla (NM_001885)	Kidan Bio	Lot#: JD-0155516-1
Plasmid: pRL-TK	Kidan Bio	Lot#: JD-M141021088-1
Plasmid: PGL3-Basic-human p53 Promoter	Kidan Bio	Lot#: JD-SG22440-1
Software and algorithms		
Graphpad Prism 8.0	Graphpad	https://www.graphpad.com/
ImageJ	Schneider et al. add1	https://imagej.nih.gov/ij/
FlowJo	BD LifeSciences	V7.6
Dockeasy platform	HOME for Researchers	https://www.dockeasy.cn/DockProtein/
Adobe Photoshop	Adobe	V2020

RESOURCE AVAILABILITY

Lead contact

Further information and requests for resources and reagents should be directed to and will be fulfilled by the lead contact, Qicai Liu (liuqicai968@smu.edu.cn).

Materials availability

This study did not generate new unique reagents.

Data and code availability

- All data reported in this paper will be shared by the lead contact upon request.
- This paper does not report original code.
- Any additional information required to reanalyze the data reported in this paper is available from the lead contact upon request.

EXPERIMENTAL MODEL AND STUDY PARTICIPANT DETAILS

Animal

All animal procedures were designed and performed according to the regulations of the Institutional Animal Care and Use Ethics Committee of Zhujiang Hospital. The establishment of LBH conventional knockout (KO) C57BL/6 mice was implemented by Cyagen Inc. via the CRISPR/Cas9 technique (contract ID: KOAI200813MG1) which generated F_0 founder animals; then, the wildtype/knockout offspring were bred, identified and maintained at the Animal Experiment Center of Zhujiang Hospital (Figure S12). Construction of the ischemia-reperfusion (I/R) injury model was performed according to a previously described method.[68] In brief, 6-week-old C57BL/6 male mice were anesthetized, intubated and ventilated. After thoracotomy, the left anterior descending coronary artery (LAD) was occluded with a 6-0 silk to achieve ischemia. After occlusion for 30 min, reperfusion was initiated by releasing the ligation. Sham-surgery mice were treated similarly except for LAD ligation and release. For LBH rescue in the hearts of LBH^{KO} mice, a total of 5×10^7 Lv5-NC or Lv5-LBH lentivirus particles injected at 4 different points near

the ligation site for each mouse 7 days prior to the I/R surgery were verified to be sufficient to induce LBH overexpression (Figure S13). All mice were sacrificed to obtain the hearts at 0, 4 or 24 h after initiating reperfusion. Each experimental group at every single time point had at least four surviving mice for sampling. Tissue sections of the left ventricles were used for western blotting, 2,3,5-triphenyltetrazolium chloride (TTC) staining or immunofluorescence staining.

METHOD DETAILS

Echocardiography (ECG)

At 24 h after reperfusion, the echocardiographic parameters of the I/R-treated mice and negative controls were measured and analyzed by a Vevo 2100 ultrasound imaging system (Visual Sonics). Specifically, the mice were anesthetized by 2% isoflurane, shaved off the chest hair and repositioned on the platform; then, assessments were performed after the mice were disconnected with the anesthesia gas machine in order to measure their ECGs under the conscious state. Under the parasternal long axis (PLAX) view in M-mode, ejection fraction (EF) and fractional shortening (FS) were measured/calculated to evaluate the left ventricular (LV) systolic function of the I/R-treated mice. For all the ECG measurements illustrated, each experimental group had at least four surviving mice for sampling. The heart rates of all measured mice in this study showed no statistical significance between any two experimental groups (Figure S14).

Isolation and culture of primary CMs

Isolation of primary CMs from neonatal LBH^{WT} or LBH^{KO} C57BL/6 mice was performed according to a previously described protocol.[69] Briefly, the left ventricles of neonatal mice were rinsed in 0.25% EDTA-trypsin at 4°C for 12 h. After inactivation of trypsinization, the tissues were digested by 0.08% collagenase II at 37°C under magnetic stirring; then, the cell suspension was placed into Petri dishes. After 2 h of incubation, the medium containing unattached cells was centrifuged, and the pellets were resuspended and cultured in complete DMEM (10% FBS, 1% penicillin-streptomycin) containing 1mM 5-bromo-2′-deoxyuridine (BrdU) for 2 days until the attached CMs pulsatile and were considered ready for the following treatment. Immunofluorescence detection of myocardium markers, including cardiac myosin, cardiac troponin T (CTnT) and α-actinin-1 (ACTN1) was performed for each batch to identify the purities of isolated CMs (Figure S15).

Lentivirus infection and cell line culture

Stable cell lines that ectopically express the LBH gene, and their corresponding negative controls were established through lentiviral infection. The myocardial cell lines H9c2 (purchased from ATCC) and AC16[70] were individually infected with Lv3-NC, Lv5-NC, Lv3-shLBH or Lv5-LBH lentivirus (all vectors integrated with eGFP reporter, Genepharma Inc.) in the presence of 0.1% v/v polybrene. After 72 h, a 2-week puromycin (2 μg/mL) screen was applied to obtain stable cell lines. AC16 cells were also used in the luciferase reporter assay and fluorescence resonance energy transfer assay during this study, which had been authenticated by short tandem repeat (STR) analysis. These H9c2 and AC16 cell lines were maintained in complete DMEM/F-12 and incubated in standard conditions (37°C and 5% CO_2). Besides, primary CMs were transiently infected with Lv3-NC, Lv5-NC, Lv3-shLBH or Lv5-LBH lentivirus (Genepharma Inc.) at the optimized multiplicity of infection (MOI), following the same procedure as the infection of H9c2 cells (Figure S16).

Hypoxia-reoxygenation treatment

Primary mouse CMs and H9c2 cell lines received hypoxia-reoxygenation (H/R) treatment to mimic the ischemia-reperfusion injury for *in vitro* detections. For hypoxic conditions, cells were cultured in glucose-free, serum-free DMEM under 1% O_2 (Forma Series 2 Incubator, Thermo Scientific) for 3 h; then, the cells were cultured in complete DMEM/F-12 under 21% O_2. Cells were sampled for following experiments at 0 h, H/R 3 + 0 h, 3 + 4 h, and 3 + 8 h respectively. The H/R time length was sufficient to induce cellular injury for both primary mouse CMs and H9c2 cells (Figure S17, Videos S1 and S2).

Reagents and compounds

The inhibitor ralimetinib was used to inhibit the phosphorylation of p38 in H9c2-LBH cells. H9c2 cells were treated with complete DMEM/F-12 containing 1 μM ralimetinib O/N before H/R treatment, which had been identified as a sufficient amount (Figure S18); 1 μM ralimetinib was also added to both glucose-free DMEM under hypoxia and complete DMEM/F-12 under reoxygenation, in order to sustain its inhibitory function. Erastin was used to mimic the ferroptosis[17] induced by H/R treatment, and DMEM/F-12 containing 10 μM erastin was identified as a sufficient amount for both primary CMs and H9c2 cells (Figure S19). Besides, the apoptosis inhibitor chloroquine diphosphate[71] and ferroptosis inhibitor ferrostatin-1[72] were introduced during the H/R process of H9c2 cells at corresponding optimized concentrations (Figures S7A and S7B), respectively.

Cellular viability assays

The cellular viabilities of lentivirus-infected H9c2 cells and primary CMs under hypoxia were assessed by using both a CCK-8 assay kit and a real-time cell analyzer (RTCA-DP) system (ACEA Biosciences, Inc.). The CCK-8 assay was performed according to the instructions from the producer, and the absorbances at 450 nm were read by a Varioskan LUX plate reader (Thermo Scientific) at designated time points. Detections using the RTCA system were modified from our published researches.[12] Briefly, after adding 50 μL of culture medium into each well on the E−16 plates, background calibrations were performed, and the operational procedures were suspended. Then, after the cells were

seeded, attached and incubated in the cradle of RTCA, the RTCA device received normoxia or H/R treatment, at which point the operational procedures were restarted. The impedance signals were recorded every 15 min until the end of the experiment. Cell index values (CIs, calculated from impedances) were applied as indicators of cellular viabilities and used for statistics.

Apoptosis detection

Because primary CMs were difficult to be properly detached for flow cytometry, TdT-mediated dUTP nick-end labeling (TUNEL) staining and Annexin V-PE/7- aminoactinomycin D (7-AAD) dual staining were applied to apoptosis detection for primary CMs and H9c2 cell lines respectively, all according to the instructions of the manufacturers. For the TUNEL assay, the samples were then stained with DAPI and imaged by a Leica DMi8 fluorescence microscope. For each group, the TUNEL positive rates of 6 different fields were measured for statistical analysis. For Annexin V/7-AAD dual staining, all stained samples were detected by a FACS Calibur flow cytometer (BD Biosciences) within 2 h. The data were analyzed by FlowJo 7.6 software, and the sums of Annexin^{+}/7-AAD^{-} and Annexin^{+}/7-AAD^{+} cells were applied to calculate the apoptosis ratios.

Ferroptosis detection

Multiple assays were applied to evaluate ferroptosis in different aspects: the total iron was measured by an iron colorimetric assay kit, and the malondialdehyde (MDA) was quantified by an MDA colorimetric assay kit for both heart tissue and cellular samples, which were detected by a Varioskan LUX plate reader; the ferrous ions (Fe^{2+}) in live cells were stained by a FerroOrange assay kit and imaged by a Leica SP8 confocal microscope.

Quantitative real-time PCR

Cells under H/R treatment or heart tissues of mice after I/R surgery were sampled with TRIzol reagent. Reverse transcription was performed with a PrimeScript RT reagent kit, and the qPCR procedure was performed with a SYBR Premix Ex Taq kit, all according to the instructions of the manufacturers. The primer sequences (synthesized by Accurate Bio Inc., China) are shown in Table S1 qPCR assays were conducted on an Applied Biosystem 7500 Fast instrument. The mRNA transcription levels of target genes were quantified by $2^{-\Delta\Delta Ct}$ method, with β-Actin as the house-keeping gene for normalization.

Western blotting

Western blotting assays were performed as previously described.[73] The antibodies used are listed in key resources table. Nuclear protein samples were separated from whole cell lysates using the NE-PER kit (Figure S20). α-Tubulin and Lamin B1 were selected as WB loading controls for cell lysates and nuclear extracts by screening to ensure that their expression was not affected by H/R treatment (Figure S21). Stripping buffer was used to retrieve the membranes between individual primary antibody incubations; membrane exposure was performed by a GE ImageQuant LAS 500 exposure instrument, while the quantifications were performed by ImageJ software.[74]

Protein-protein interaction (PPI)

Protein-protein interaction (PPI) between p53 and phospho-CRYAB protein in cardiomyocytes was evaluated by the combination of molecular docking, co-immunoprecipitation (co-IP) and fluorescence resonance energy transfer (FRET). Rigid protein-protein docking (ZDOCK) between CRYAB and p53 proteins was performed on the Dockeasy platform (https://www.dockeasy.cn/DockProtein). The PDB format of the protein structural domain was downloaded from the Protein DataBank PDB database (http://www.rcsb.org/). The ZDOCK module was run to identify the docking sites and calculate the ZDOCK scores. The co-IP assay was performed by protein A/G magnetic beads (Bimake, B23202), all according to the instructions of the manufacturers, during which both mouse-*anti*-p53 and rabbit-*anti*-phospho-CRYAB were bound to magnetic beads to detect the PPI between p53 and phospho-CRYAB. For the FRET assay, the following plasmids were constructed: pCDH-CMV-TP53-gfp-EGFP-EF1-Puro for expressing p53-eGFP, and pLV-CMV-CRYAB-mCherry-6His-IRES-Bla for expressing CRYAB-mCherry. Correspondingly, the pCDH-CMV-gfp-EGFP-EF1-Puro and pLV-CMV-mCherry-6His-IRES-Bla plasmids were used as negative controls. According to the requirements for the sensitized emission (SE) method, 4 groups were established for plasmid transfection with Lipofectamine 3000 reagent: negative control, donor (p53-eGFP) only, acceptor (CRYAB-mCherry) only, which were designed for calibrations, and the dual-transfected group for the FRET assay. The calculations of FRET efficiencies were performed by the FRET-SE module of the Leica SP8 microscope based on an established formula[75]:

$$EA(i) = [B - A*\beta - C*(\gamma - \alpha*\beta)] / [C*(1 - \beta*\delta)]$$

A = Donor channel, B=FRET channel, C=Acceptor channel; α = A/C, β = B/A, γ = B/C,δ = A/B.

Immunofluorescence staining

Cell samples seeded on round coverslips (Electron Microscope Sciences, 12 μm) were then fixed with 4% PFA for 10 min. Tissue sections received deparaffinization (Histoclear, National Diagnostics), rehydration and sodium citrate antigen retrieval. All samples were blocked with goat serum for 30 min, incubated with primary antibodies O/N at 4°C and then incubated with fluorescence-conjugated secondary antibodies at room temperature for 2 h. Then, DAPI was applied to stain the nuclei and the samples were mounted onto glass slides and imaged

by a Leica DMi8 fluorescence microscope or a Leica SP8 confocal microscope. The antibodies used are listed in key resources table. The whole-slide images of mounted tissue sections were photographed by a GE Amersham Typhoon imager, all according to our previous protocol.[13]

Dual-luciferase reporter assay

Before the experiment, the sequence of previously reported human p53 gene promoter[76] was inserted into the pGL3-Basic vector. Then, AC16 cells, AC16-Lv3NC, AC16-Lv5NC, AC16-LBH or AC16-shLBH cell lines were co-transfected with this constructed vector and the pRL-TK vector by Lipofectamine 3000 reagent. 36 h later, transfected AC16 primary cells received H/R treatments. The H/R treated AC16 primary cells, together with constructed AC16 cell lines were sampled and applied to a dual-luciferase reporter assay kit, all according to the instructions of the manufacturers. Finally, the samples reacted with Firely/Renilla luciferase were placed into 96-well white plates (Corning #3912) and read by the chemiluminescence module of a Varioskan LUX plate reader (Thermo Scientific). The transcriptional activity of the p53 gene in treated AC16 cells was indicated by the relative Firely luciferase activity calibrated by Renilla luciferase activity and the blank control.

QUANTIFICATION AND STATISTICAL ANALYSIS

The data presented were collected from three independent, parallel experiments and are presented as the mean ± SD. Statistical analysis was conducted using unpaired Student's t-tests and one-way ANOVA (Brown-Forsythe test), with GraphPad Prism software V8.0. p values <0.05 were considered statistically significant.